Effect of dietary monosodium glutamate on *trans* fat-induced nonalcoholic fatty liver disease

Kate S. Collison,[1] Zakia Maqbool, Soad M. Saleh, Angela Inglis, Nadine J. Makhoul, Razan Bakheet, Mohammed Al-Johi, Rana Al-Rabiah, Marya Z. Zaidi, and Futwan A. Al-Mohanna

Cell Biology and Diabetes Research Unit, Department of Biological and Medical Research, King Faisal Specialist Hospital and Research Centre, Riyadh 11211, Saudi Arabia

Abstract **The effects of dietary monosodium glutamate (MSG) on *trans*-fatty acid (TFA)-induced nonalcoholic fatty liver disease (NAFLD) are addressed in an animal model. We used Affymetrix microarray analysis to investigate hepatic gene expression and the contribution of visceral white adipose tissue (WAT) to diet-induced NAFLD. *Trans*-fat feeding increased serum leptin, FFA, HDL-cholesterol (HDL-C), and total cholesterol (T-CHOL) levels, while robustly elevating the expression of genes involved in hepatic lipogenesis, including the transcription factor sterol-regulatory element binding protein 1c. Histological examination revealed hepatic macrosteatosis in TFA-fed animals. Conversely, dietary MSG at doses similar to human average daily intake caused hepatic microsteatosis and the expression of β-oxidative genes. Serum triglyceride, FFA, and insulin levels were elevated in MSG-treated animals. The abdominal cavities of TFA- or MSG-treated animals had increased WAT deposition compared with controls. Microarray analysis of WAT gene expression revealed increased lipid biosynthetic gene expression, together with a 50% decrease in the key transcription factor Ppargc1a. A combination of TFA+MSG resulted in the highest levels of serum HDL-C, T-CHOL, and leptin. Microarray analysis of TFA+MSG-treated livers showed elevated expression of markers of hepatic inflammation, lipid storage, cell damage, and cell cycle impairment. TFA+MSG mice also had a high degree of WAT deposition and lipogenic gene expression. Levels of Ppargc1a were further reduced to 25% by TFA+MSG treatment.** **MSG exacerbates TFA-induced NAFLD.**—Collison, K. S., Z. Maqbool, S. M. Saleh, A. Inglis, N. J. Makhoul, R. Bakheet, M. Al-Johi, R. Al-Rabiah, M. Z. Zaidi, and F. A. Al-Mohanna. **Effect of dietary monosodium glutamate on *trans* fat-induced nonalcoholic fatty liver disease.** ***J. Lipid Res.*** **2009.** 50: **1521–1537.**

Supplementary key words *trans*-fatty acid • triglycerides • free fatty acids • mitochondria • peroxisomes • microsomes

Nonalcoholic fatty liver disease (NAFLD), the most common hepatic disorder of industrialized countries, affects approximately 15–25% of the general population (1). Previously unrecognized until the early 1980s, NAFLD is a progressive disease with an etiology related to recent changes in diet and lifestyle. In a number of cases, patients go on to develop nonalcoholic steatohepatitis (NASH), a more severe disease associated with obesity, insulin resistance (2), and mitochondrial dysfunction (3). Estimations of the incidence of NASH in the general population vary from 2–3% (4), with indications that this condition is becoming increasingly prevalent even in the pediatric population (5), who are nearly always insulin resistant regardless of body mass index (6). Insulin resistance is a common occurrence in obesity, metabolic syndrome, and type 2 diabetes and can be induced experimentally by high-fat diets (7). Since 1970, consumption of oils and fats in the US has increased by 62% (8), with vegetable oil assuming a larger percentage of total fat intake. *Trans*-fatty acids (TFAs) derived from vegetable oils and shortenings now accounting for between 1.7% and 8% of the world dietary fat consumption (9). TFA ingestion promotes obesity, decreases insulin sensitivity (10), and increases the risk of cardiovascular disease in the general population (11). Central obesity and insulin resistance can also be induced experimentally via ablation of the arcuate nucleus using neonatal administration of a high dose(s) of the food flavor enhancer monosodium glutamate (MSG) (12–14).

This work was supported by Research Advisory Council Project 2070 006, King Faisal Specialist Hospital and Research Centre.

Manuscript received 5 August 2008 and in revised form 27 October 2008 and in re-revised form 11 November 2008.

Published, JLR Papers in Press, November 11, 2008
DOI 10.1194/jlr.M800418-JLR200

Abbreviations: AA, arachidonic acid; Acly, ATP citrate lyase; Ahr, aryl hydrocarbon receptor; bw, body weight; CYP7A1, cholesterol 7α-hydroxylase; Cyp, Cytochrome P450; Fasn, fatty acid synthase; HDL-C, high density lipoprotein cholesterol; Fmo2, flavin-containing monooxygenase 2; HE, hematoxin-eosin; Hsd3b, 3-hydroxy-3-methylglytaryl-CoA synthase; MSG, monosodium glutamate; MTTP, microsomal triglyceride transfer protein; NAFLD, nonalcoholic fatty liver disease; NASH, nonalcoholic hepatic steatosis; qRT-PCR, quantitative reverse transcription polymerase chain reaction; RBP4, Retinol Binding Protein 4; REDOX, reduction/oxidation reaction; SREBP1c, sterol-regulatory element binding protein 1c; T-CHOL, total cholesterol; TFA, *trans*-fatty acid; TG, triglyceride; WAT, white adipose tissue.

[1]To whom correspondence should be addressed.
e-mail: kate@kfshrc.edu.sa

The mechanism for this is believed to involve glutamate-induced degeneration of those areas of the immature brain that are insufficiently protected by a mature blood-brain barrier, including regions that regulate feeding and satiety (15). MSG consumption has increased globally in recent years, with recent estimations of the current average daily intake believed to be up to 10 g/day (16). In 1974, an acceptable daily intake for MSG was set at 0–120 mg/kg body weight (bw) (17). In Europe, intake of MSG consumption is estimated as approximately 30 mg/kg bw (18), although in some countries, intake of MSG could be as high as 143 mg/kg bw (16). In addition to obesity and dyslipidemia, recent data suggest that MSG may cause hepatic steatosis (19), inflammation, and dysplasia (16); however, the mechanism behind this is incompletely understood. The aim of this work was to establish the effect of dietary TFA and MSG on dyslipidemia, hepatic steatosis, and gene expression profile and to assess the role of visceral white adipose tissue (WAT) in the pathogenesis of nonalcoholic fatty liver disease using an in vivo animal model. The amount of low-dose oral MSG used in this study (91 mg/kg bw) reflects current consumption levels (17, 18) and is 30–40 times less than the level previously reported to induce neuronal damage when injected neonatally (13–15). Since it has previously been suggested that MSG excitotoxicity occurs only when the blood brain barrier is vulnerable, for example, neonatally (15), we studied C57Bl/6J mice that had been bred and weaned from animals maintained on the respective diets for a 3-week run-in period prior to mating. We analyzed hepatic and WAT microarray gene expression in order to gain insight into the commonalities and differences between the mechanism of TFA-induced steatosis versus that induced by MSG. To our knowledge, this is the first article to address the effect of these common food substances on hepatic and WAT gene expression in a rodent model of NAFLD.

EXPERIMENTAL PROCEDURES

Animals and diets

C57BL/6J mice were from The Jackson Laboratory (Maine) and were housed/caged and fed a standard chow diet until 6 weeks of age, whereupon they were placed in one of four different dietary regimens for a period of 3 weeks prior to mating. The four diet regimens used in this study were as follows: *1*) ad lib standard chow (control diet) with ad lib drinking water; *2*) ad lib standard chow with ad lib drinking water containing 0.64 g/l (91.2 ± 4.6 mg/kg bw):MSG(MSG diet); *3*) ad lib test diet Purina 5001 with 20% (w/w) partially hydrogenated vegetable shortening [Test Diet #5C4M containing 8.68% (w/w) TFAs; Test Diet Purina] and ad lib drinking water (TFA diet); and [4] Diet #5C4M and ad lib drinking water containing 0.64 g/l (97 mg/kg bw) MSG (TFA+MSG diet). See Table 1 for diet composition. Following mating, the four groups of dams were maintained on their respective diets throughout the gestation and nursing period. Male offspring used in these experiments were weighed and then weaned onto the same diets and maintained in this regimen until they reached either 16 or 32 weeks of age. Average body weight and caliper girth was assessed at 6, 16, and 32 weeks of age; water intake and food consumption were assessed at 6 weeks and again at 28–30 weeks. The breeding and care of the animals were in accordance with the protocols approved by the Animal Care and Use Committee of the King Faisal Specialist Hospital and Research Centre.

Measurement of murine serum triglycerides, FFAs, cholesterols, fasting glucose, insulin, adiponectin, leptin, and RBP4 levels

Serum triglyceride (TG), total cholesterol (T-CHOL), and HDL-cholesterol (HDL-C) concentrations were measured in overnight fasted male 32-week-old mice (n = 20) using the Reflovert Plus instrument (Roche, F. Hoffmann-La Roche, Basel, Switzerland) according to the manufacturer's instructions. Overnight fasting blood glucose was measured using the Ascensia Contour glucometer (Bayer HealthCare, IN). FFAs were measured in mouse serum using the Half Micro Test (Roche Diagnostics, Mannheim, Germany). Hormone measurements were also taken at 32 weeks of age. Fasting serum insulin was measured using the ultrasensitive mouse insulin ELISA kit from Mercodia (Uppsala, Sweden) according to the manufacturer's instructions. Fasting serum leptin and adiponectin/Acrp30 were measured by ELISA using commercial assay kits (MRP300 mouse Adiponectin/Acrp30; MOB00 mouse leptin, R and D Systems, Minneapolis, MN). Fasting serum Retinol Binding Protein 4 (RBP4) was measured using the Dual mouse/rat RBP4 ELISA kit (RB0642EK; AdipoGen, Seoul, Korea).

Histology and Oil-Red-O staining of murine liver and adipose tissue

Liver and visceral adipose tissues were removed and weighed. Formalin-fixed, paraffin-embedded liver and adipose tissue from eight of the 32-week-old male mice were processed, and 4-μm-thick serial sections were cut and stained with Oil-Red-O or hematoxylin and eosin (HE) for lipid analysis according to standard pathology laboratory procedures. After mounting with glycerol gelatin, images were captured using Axio Vision Rel4.5 software (Carl Zeiss). For measurement of adipocyte cell areas, images were converted to TIFF files for analysis using the Discovery Series™ Quantity One® 1-D analysis software (Bio-Rad Laboratories).

Hepatic TG quantitation

Levels of mouse liver TG were quantified using the Triglyceride Determination Kit TRO100 with appropriate TG standards (Sigma-Aldrich, St. Louis, MO). Frozen liver samples from 32-week-old mice were first powdered under liquid nitrogen and 120 mg of the frozen liver powder was weighed into 2 ml of chloroform:methanol mix (2:1, v/v) and incubated for 2 h at room temperature with occasional shaking. Following the addition of 0.2 volumes of water, vortexing, and centrifuging at 2,500 *g*, the lower phase containing the lipids was collected and dried under vacuum in a rotary evaporator for 5–6 h. The dried pellets were resuspended in the reaction buffer provided in the kit. Results were expressed as mean TG (mg/g tissue) ± SEM, n = 6 per diet group.

RNA isolation

To detect early changes in gene expression, total RNA was prepared from the liver and visceral adipose tissue taken from 16-week-old mice (n = 4) in the four different diet groups using the Qiagen RNeasy kit according to the manufacturer's instructions and stored at −80°C. RNA quality was verified using a 2100 Bioanalyzer instrument and an RNA 6000 Nano LabChip assay (Agilent Technologies, Santa Clara, CA). RNA concentrations were determined by absorption at 260-nm wavelength with an ND-1000 spectrometer (Nanodrop Technologies, Wilmington, DE).

Liver/adipose samples were pooled into two samples per diet group and applied onto two microarray chips, giving a total of n = 4 samples.

Microarray hybridization

Gene expression in these samples was analyzed using GeneChip Mouse Gene 1.0 ST array. A high-density oligonucleotide microarray (Affymetrix, CA) representing 28,853 genes, with approximately 27 probes spread across the full length of each transcript, was used. Targets were prepared and microarrays were processed as described in the Affymetrix GeneChip Whole Transcript Expression Analysis manual using the commercially available Affymetrix GeneChip WT cDNA synthesis kit, WT cDNA amplification kit, and WT Terminal labeling kit as per the manufacturer's instructions. Briefly, approximately 200 ng of total RNA was used to synthesize double-stranded DNA with random hexamers tagged with a T7 promoter sequence. The cDNA was used as a template for in vitro transcription. In the second cycle of cDNA synthesis, random primers were used in reverse transcription to convert the cRNA into single-stranded DNA, which was fragmented, labeled, and hybridized to the array for 16 h using the Fluidics 450 station. Arrays were scanned using the Affymetrix 3000 7G scanner and GeneChip Operating Software version 1.4 to produce CEL intensity files. This software also provided summary reports by which array QA metrics were evaluated, including average background, average signal, and 3′/5′ expression ratios for spike-in controls, β-actin, and GAPDH.

Real-time RT- PCR

Confirmation of microarray results was performed by quantitative real-time RT-PCR (qRT-PCR) on independently derived mRNAs from the livers of a different set of four 16-week-old mice per diet group. RNA quality was verified using a 2100 Bioanalyzer instrument and an RNA 6000 Nano LabChip assay (Agilent Technologies, Palo Alto, CA). Total RNA (2 μg) was reverse transcribed using Promega Reverse Transcription system (Promega, Madison, WI).

Primers

Gene-specific primers corresponding to the PCR targets were designed using the Primer 3 program. The following oligonucleotides were selected: cell death-inducing DFFA-like effector c (CIDEC) forward 5′-AGCTAGCCCTTTCCCAGAAG-3′ and reverse 5′-CCTTGTAGCAGTGCAGGTCA-3′; Cyp7A1 forward 5′-ACACCATTCCTGCAACCTTC-3′ and reverse 5′-GCTGTCCGGATATTCAAGGA-3′; GADD45b forward 5′-CTCCTGGTCACGAACTGTCA-3′ and reverse 5′-GGGTAGGGTAGCCTTTGAGG-3′; microsomal triglyceride transfer protein (MTTP) forward 5′-GAGGCTGGGCTGGAGTTCAT-3′ and reverse 5′-ACCGGAGTTATCGCTTTCTG-3′; sterol-regulatory element binding protein 1c (SREBP1c) forward 5′-GATCAAAGAGGAGCCAGTGC-3′ and reverse 5′-TAGATGGTGGCTGCTGAGTG-3′; β-Actin forward 5′-AGCCATGTACGTAGCCATCC-3′ and reverse 5′-CTCTCAGCTGTGGTGGTGAA-3′. Conditions for real-time PCRs were first optimized using a gradient Cycler (Bio-Rad Laboratories, CA). RT-PCR amplification product were separated on 2% agarose gel and analyzed with the Quantity One 1-D Software (Bio-Rad Laboratories). Optimized conditions were transferred to the LightCycler real-time PCR protocol. $MgCl_2$ concentrations were reoptimized using the LightCycler protocol (Roche Molecular Biochemicals, Mannheim, Germany). Preliminary real-time RT-PCR experiments were performed with each primer pair to determine the annealing temperature that yielded the greatest amount of specific product with melting temperature separable from primer-dimer temperature.

Relative standard curves and PCR assay conditions

Standard curves were prepared for each run using known quantities of cDNA (10-fold dilutions beginning at 15 ng/μl) and primers for the gene of interest or β-actin. Light Cycler-Fast Start DNA Master SYBR Green I reaction mix containing 0.4 μM forward and reverse primers, 4 M $MgCl_2$, and 1 μl LightCycler-Fast start DNA master SYBR Green 1 dye was used for quantitative real-time PCR analysis according to the manufacturer's protocols (Roche Molecular Biochemicals, Mannheim, Germany). A volume of 1 μl from a 10-fold dilution of cDNA was added as the PCR template. A no-target control received 9 μl reaction mix and 1 μl water. PCR amplification was performed in triplicate wells. A four-step experimental run protocol was performed: *i*) denaturation program (10 min at 95°C); *ii*) 45 cycles of four-segment amplifications consisting of denaturation at 95°C for 10 s, annealing (60–56°C) for 5 s, extension at 72°C for 10 s, and data acquisition at 83°C for 1 s. A temperature transition rate of 2°C/s with a single fluorescence measurement was used. *iii*) Melting curve program (50–95°C, with heating rate of 0.1°C/s up to 98°C with continuous fluorescence measurement); and *vi*) a cooling program down to 40°C. Relative quantitation measurements were performed using external standard curves for both target and β-actin housekeeping gene. The second derivative maximum method was used for cycle threshold (ct) calculation from amplification curves. The respective concentration for any given sample was calculated using crossing-cycle analysis provided by the LightCycler software.

Statistics

Microarray data analysis was performed with the Partek genomic suite software suite 6.3 (Partek, MO). Probe set data were summarized, background adjusted, and quantile normalized using robust multichip average methodology described in Irizarry et al. (20). A false discovery rate correction was applied to post hoc pairwise group comparisons of Pearson's correlation coefficients obtained by ANOVA. Heat map and clustering of the gene expression data were also generated using Partek. $P \leqslant 0.05$ was considered significant, with an arbitrary threshold of 1.5-fold difference between the four groups analyzed simultaneously. As the mRNA expression in four animals from each of the four diet groups was separately analyzed, four comparisons were possible when comparing the effects of TFA diet animals with respect to controls receiving standard chow and the effect of the addition of MSG to both diets. Genes fulfilling the Affymetrix quality criteria for significant expression were considered to be differentially expressed between the four diet groups when the expression levels were concordantly increased or decreased in all four comparisons. Real-time RT-PCR values for each target gene were calculated as a ratio of target gene expression level to the β-actin expression level in the same specimen. For concordance comparisons with the microarray data, these values were then expressed as mean percentage ± SEM of real-time RT-PCR levels in the control diet group. *P* values of <0.05 were considered statistically significant. Pearson correlation coefficients (*r*) between the microarray data and the qRT-PCR were calculated. A value of 1 is indicative of a perfect correlation.

SREBP1c activity measurement

SREBP1c activity was determined in nuclear fractions of liver using the ELISA-based SREBP1 activation TransAM kit (Active Motif, CA). The Trans-AM SREBP1 kit contained a 96-well plate on which an oligonucleotide containing a sterol-responsive ele-

ment specific for SREB1c had been immobilized. SREBP1c contained in nuclear extracts (10 μg liver extracts from four mice per diet group) specifically bound to this oligonucleotide and was detected by addition of a primary antibody that recognized an accessible epitope on SREBP1 protein upon DNA binding. The specificity of this assay was assessed by incubating the nuclear extract with 5 pmol/well of a wild-type consensus oligonucleotide provided in the kit, which competes with the nuclear extract SREBP1 for the immobilized probe on the assay plate. Addition of a secondary horseradish peroxidase-conjugated antibody provided a colorimetric readout quantified by spectrophotometry (450 nm). Results were expressed as mean OD (450 nm) ± SEM (n = 4).

RESULTS

Diets and nutritional parameters

Table 1 lists percentages of dietary components with respect to weights of the fresh materials. Daily food and water intake was not significantly different within the four diet groups. MSG was added to the drinking water at a final concentration of 0. 64 g/l so as not to influence food consumption. Averaged daily MSG intake was 91.21 ± 4.63 mg/kg bw. Initial and final body weight were comparable between the four groups; however, the percentage weight changes between 6 and 32 weeks differed significantly, with the MSG-treated groups achieving a lower growth rate and TFA diets achieving the largest increase in body weight $P \leq 0.05$, n = 20 (**Table 2**). The overall difference in weight change between the four diet groups was highly significant ($P \leq 0.001$). Abdominal girth was markedly increased in the TFA+MSG group ($P \leq 0.001$), with a maximum girth increase of 52.1 ± 2.5% occurring between 6 and 32 weeks of age.

Lipid metabolism, serum glucose, insulin, and adipokine profile

Total TG, FFA, and HDL-C were increased significantly in all three diet groups compared with control (Table 2; $P = 0.0402$, $P \leq 0.0001$, and $P = 0.0022$, respectively). The highest levels of serum TG, T-CHOL, and HDL-C were found in the TFA+MSG group, with increases of 39.3, 10.5, and 42.8%, respectively ($P \leq 0.05$). Fasting blood glucose, insulin, leptin, adiponectin, and RBP4 were measured (Table 2). There was no significant difference in fasting glucose and adiponectin levels. Fasting insulin was significantly elevated in the MSG group ($P < 0.05$, n = 6). Serum leptin levels were markedly elevated in the TFA and TFA+MSG diet groups ($P = 0.0138$, n = 6). Conversely, serum levels of RBP4 were elevated in all three diet groups relative to control ($P \leq 0.001$).

TABLE 1. Composition of experimental diets

Ingredients (g/100 g dw)	Control	MSG	TFA	TFA+MSG
Protein (%)	22.50	22.50	19.10	19.10
Carbohydrate (%)	64.20	64.20	37.70	37.70
Fat (%) (ether extract)	5.00	5.00	28.00	28.00
Fiber	3.00	3.00	4.30	4.30
Vitamins, minerals, and ash	5.30	5.30	10.90	10.90
Energy (kcal/g)	3.36	3.36	4.39	4.39
MSG (mg/kg bw) provided in drinking water	0.00	91.21	0.00	91.21

Hepatic histology, lipid staining, and TG content

Increased hepatic lipid deposition as depicted with Oil-Red-O staining was apparent in 32-week MSG- and TFA-treated animals compared with control (**Fig. 1A**). The livers of TFA-treated animals contained larger vesicular structures consistent with macrovesicular steatosis (Fig. 1A, B). Conversely, microvesicular steatosis was apparent in the livers of MSG-treated animals, as indicated by Oils-Red-O (Fig. 1A) and HE staining (Fig. 1B) of mouse liver tissue. Interestingly, in the TFA+MSG animals, microvesicular steatosis was predominant, and there was an attenuation of macrovesicular structures in the livers from this diet group (Fig. 1B). Higher magnification revealed an increase in hepatic cell volume and nuclear size in MSG-treated livers (Fig. 1C). While the weight of livers from control, MSG, and TFA diet group mice did not differ significantly, livers from TFA+MSG-treated mice weighed an average 1.54-fold higher than control (Fig. 1D; $P \leq 0.05$, n = 10). Intrahepatic TG levels were quantified (Fig. 1E). The highest level of hepatic TG occurred in the TFA diet group with a 1.43-fold increase in hepatic lipid content compared with control (Fig. 1E; $P \leq 0.05$, n = 6).

Hepatic gene expression

To detect early changes in gene expression that might account for the hepatic steatosis and dyslipidemia seen in 32-week-old mice, total RNA samples were isolated from liver tissue obtained from four individual 16-week-old mice from each of the diet groups and pooled (n = 2) for applying onto two individual Affymetrix Mouse Genome 1.0 ST Array Expression Set GeneChips containing 28,853 genes. Statistical analysis of these two sets of paired samples using a *t*-test ($P \leq 0.05$, n = 4) identified a group of 84 hepatic genes whose expression was significantly changed within the four diet groups. **Figure 2** shows the heat map and clustering dendogram of the differentially expressed genes. **Table 3** shows 84 genes falling into 12 different functional ontologies, which were differentially expressed within the four groups, using a 1.5-fold change as a significance threshold ($P \leq 0.05$). The expression of genes involved in lipid biosynthesis, storage, and catabolism was most significantly affected by the different diets compared with control. The greatest effect on hepatic gene expression was seen in the TFA diet, where the expression of 21 genes involved in lipid biosynthesis was markedly upregulated (Table 3; $P \leq 0.05$). Key regulatory protein SREBP1c, known to control the expression of a number of lipogenic genes (21), was also increased by the TFA diet by 2.5-fold. Other biosynthetic genes included 3-hydroxy-3-methylglytaryl-CoA synthase (3.6-fold), Fatty acid synthase (Fasn; 2.4-fold), and ATP citrate lyase (Acly; 1.6-fold). Interestingly, the expression of many TFA-induced lipogenic genes was decreased to control levels by the combination

TABLE 2. Metabolic characteristics and food/water intake of study subjects

	Control	MSG	TFA	TFA+MSG
Initial body weight (g)	18.82 ± 2.42	19.18 ± 1.43	17.18 ± 1.87	18.18 ± 1.43
Weight at 32 weeks (g)	29.58 ± 2.49	27.89 ± 1.83	34.38 ± 4.05	34.04 ± 5.18
Weight change (%)	58.69 ± 2.51^{a}	45.41 ± 1.83^{b}	79.72 ± 2.3^{c}	75.55 ± 3.18^{c}
Girth change (%)	30.59 ± 1.54^{bc}	36.94 ± 1.45^{b}	29.23 ± 2.2^{c}	52.08 ± 2.5^{a}
Daily food intake (g)	2.77 ± 0.07	3.21 ± 0.11	2.76 ± 0.34	2.76 ± 0.13
Daily water intake (ml)	3.94 ± 0.55	4.54 ± 0.12	4.43 ± 0.43	4.95 ± 0.63
Glucose (mg/dl)	52.76 ± 10.73	53.39 ± 8.40	76.27 ± 18.93	60.0 ± 14.12
Insulin (ng/ml)	0.34 ± 0.02^{a}	0.57 ± 0.04^{b}	0.42 ± 0.03^{ab}	0.53 ± 0.08^{ab}
Leptin (ng/ml)	2.35 ± 0.30^{a}	2.38 ± 0.98^{a}	9.24 ± 2.07^{ac}	11.33 ± 3.70^{bc}
Adiponectin (μg/ml)	3.42 ± 0.50	4.37 ± 1.12	4.65 ± 5.14	5.95 ± 1.11
RBP4 (μg/ml)	25.33 ± 0.04^{a}	28.25 ± 0.18^{b}	32.45 ± 0.06^{c}	30.23 ± 0.10^{d}
TG (mg/dl)	80.93 ± 7.79^{a}	132.13 ± 12.63^{b}	98.60 ± 11.1^{ab}	112.70 ± 14.87^{ab}
FFA (μM)	5 ± 0.22^{a}	427 ± 40^{ba}	318 ± 21^{bc}	298 ± 32^{c}
HDL-C (mg/dl)	59.18 ± 5.34^{a}	69.95 ± 2.53^{b}	80.80 ± 5.44^{b}	84.53 ± 3.26^{b}
T-CHOL (mg/dl)	119.2 ± 2.92^{a}	118.0 ± 1.45^{a}	124.67 ± 3.41^{ac}	131.67 ± 1.17^{bc}

Initial and 32-week body weight, weight change (6–32 weeks), girth change (6–32 weeks), food and water intake, together with fasting serum TG in 32-week-old male C57Bl/6J mice (mean ± SEM, n = 20). FFA, HDL-C, T-CHOL fasting serum insulin, and adipokine levels in 32-week-old male C57BL/6J mice (mean ± SEM, n = 6). For statistical significance, means that are not denoted with a common letter are different: a, b, c, and d, $P < 0.05$ by ANOVA.

of dietary TFA+MSG, including Acly, Fasn, Insulin induced gene 1, and Hydroxy-δ-5-steroid dehydrogenase 3β (Hsd3b2 and Hsd3b3). The TFA diet also increased the expression of other genes involved in cholesterol synthesis, such as Farnesyl Diphosphate Synthase (6.7-fold) and Farnesyl Diphosphate Farnesyl Transferase 1 (3-fold); however, the addition of MSG to the TFA diet again reduced expression by approximately one-third. MSG markedly induced the expression of catabolic genes, including microsomal β-oxidative Cyp2b9 and Cyp2b10 (4.4- and 5.1-fold, respectively), and arachidonic acid (AA)-metabolizing Cyp2c55 (2.3-fold). Hepatic expression of these three monooxygenases was also highly upregulated by the TFA diet (7.3-, 7.0-, and 3.5-fold), and unlike the situation with the genes involved in lipid biosynthesis, hepatic expression of these catabolic proteins remained high in the TFA+MSG diet. A second microsomal oxidative protein, flavin-containing monooxygenase 2 (Fmo2) and its transcriptional regulator aryl hydrocarbon receptor (Ahr) were also upregulated in MSG-treated livers (2.3- and 1.6-fold, respectively) but remained unaffected by the other diets. This suggests that part of the effect of MSG in the liver is to increase hepatic lipid catabolism via upregulation of oxidative genes. Additionally, MSG activated genes involved in the bile acid pathway included key regulatory enzyme cholesterol 7α-hydroxylase (CYP7A1), which was increased by 2.5-fold. This was accompanied by a 1.8-fold decrease in expression of the nuclear receptor SHP, part of the negative transcriptional regulators of classical bile acid synthesis (22).

Lipid mobilization and storage processes were most affected in livers from the TFA+MSG diet group. Fat-Specific Protein 27 (CIDEC), known to be associated with lipid droplet formation (23), was upregulated by both the MSG diet and the TFA+MSG diet relative to control (1.9- and 4.0-fold, respectively) but unaffected by TFA alone (Table 3; $P < 0.05$). Ketogenic Fibroblast Growth Factor 21, a key mediator of hepatic lipid mobilization, was induced 2.4-fold. Additionally, expression of genes associated with hepatic fibrosis, including β-laminin (Lamb3b) and γ-actin (Actg1), were increased in the TFA+MSG livers by 1.9- and 1.5–fold, respectively (Table 3; $P \leqslant 0.05$). The MSG diet induced an increase in the expression of a number of key transcriptional regulatory proteins, including Growth Arrest and DNA damage-inducible 45B (GADD45b; 2.7-fold) and NIPA-like domain containing 1 (2.3-fold); in each case, expression returned to control levels in animals treated with the TFA+MSG diet. The TFA+MSG diet also induced the expression of genes involved in the inflammatory pathway, including a 1.4-fold increase in Interferon-α 14, a 7.5-fold increase in adipsin (complement factor D), and a 2-fold increase in defensin β1. Hepatic expression of apoptotic regulator p21 was increased by 2.4-fold in the TFA+MSG diet, further suggestive of a link between oxidative stress, inflammation, and cell cycle impairment in this model of diet-induced NAFLD.

Confirmation of Affymetrix microarray by real-time qRT-PCR

A set of five genes was randomly selected for validation via real-time qRT-PCR using mRNA derived from mice other than those used for the microarray study (n = 4 per diet group). **Figure 3A** shows qRT-PCR analysis of hepatic expression of CIDEC (NM_178373), cyp7a1 (NM_007824), GADD45b (NM_008655), MTTP (NM_008642), and SREBP1c (NM_011480) levels relative to housekeeping β-actin levels in mice from the four different diet groups (n = 4, $P < 0.05$). Figure 3B shows representative ethidium bromide-stained RT-PCR products electrophoresed on 2% agarose gels. Figure 3C shows concordance of qRT-PCR results versus microarray results expressed as signal intensity (percentage control diet ± SD). Pearson correlation coefficients (r) are indicated on each graph. Values of r were >0.9 in all cases, suggesting a high level of agreement between the microarray and the qRT-PCR data. Individual values were as follows: CIDEC, 0.99; Cyp7a1, 0.99; GADD45b, 0.99; MTTP, 0.99; and SREBP1c, 0.96 ($P < 0.05$).

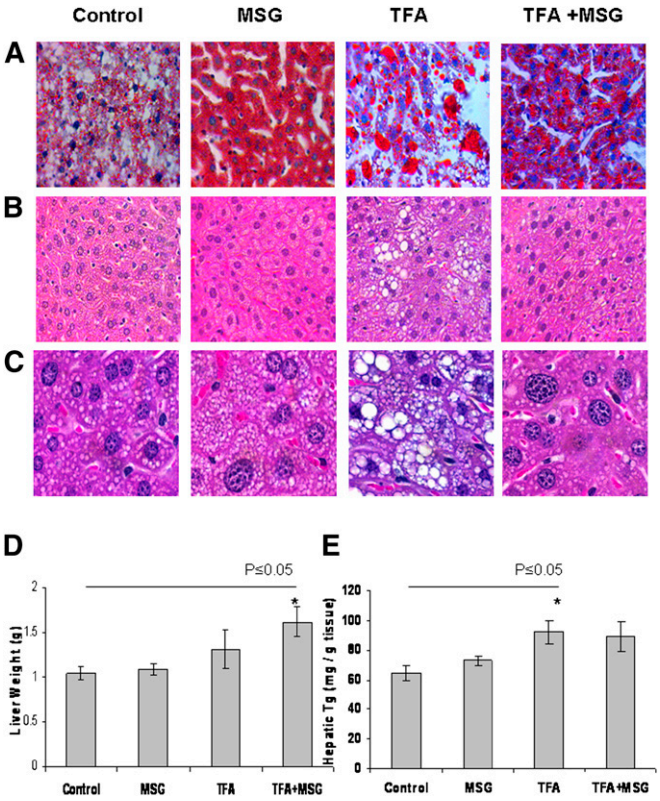

Fig. 1. Diet-induced changes in liver histology and TG content. A: Increased lipid deposition, as indicated by Oil-Red-O lipid staining in liver sections from mice on the MSG, TFA, and TFA+MSG diet groups at 32 weeks, compared with control. Red staining indicates lipid deposition. Scale is ×790. Micrographs are representative of five different experiments per diet group. B: Microvesicular steatosis in HE-stained liver sections. Scale is ×790. Micrographs are representative of five different experiments per diet group. C: Higher-magnification micrographs. D: Liver weight differences among the four different diet groups. Results are mean ± SEM ($P \leqslant 0.05$, n = 6). E: Quantitation of hepatic TG content from mice in the control (standard chow), MSG, TFA, and TFA+MSG diet groups. Results are mean ± SEM ($P \leqslant 0.05$, n = 6).

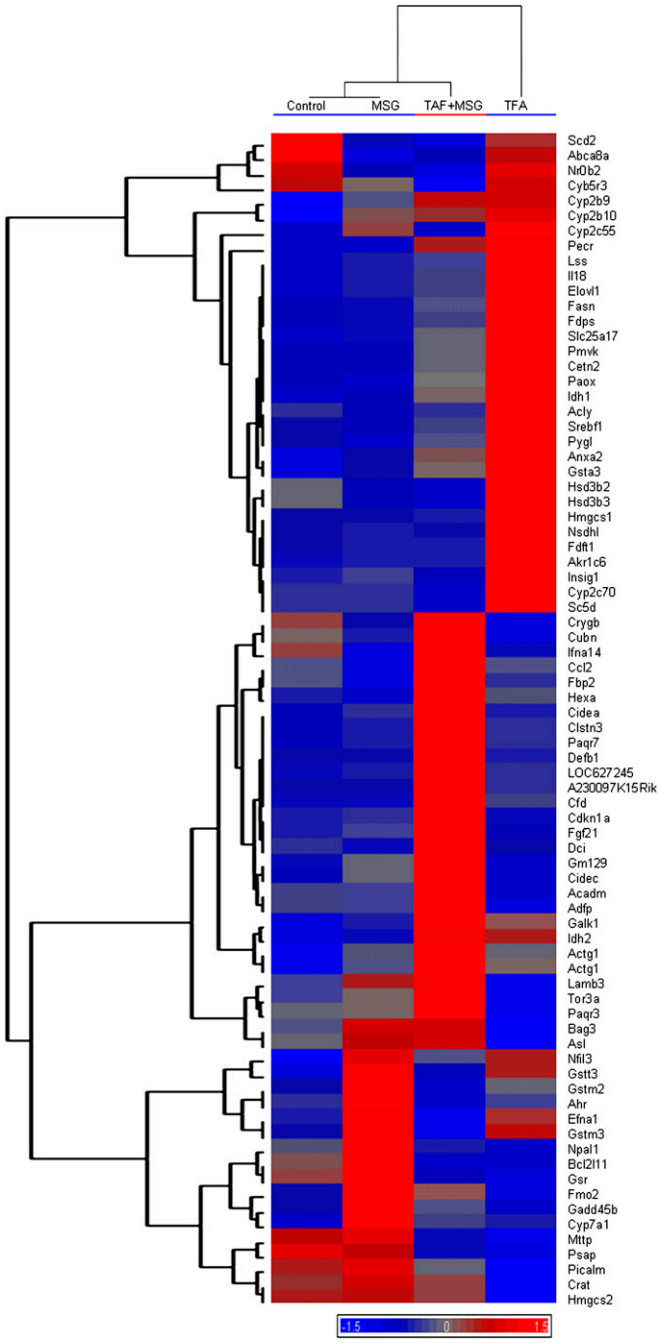

Fig. 2. Liver expression heat map and unsupervised hierarchical clustering analysis. Red pseudocolor and blue represents upregulated and downregulated genes, respectively. Each row represents a differentially expressed gene within livers from mice in the four diet groups ($P \leqslant 0.05$). Each column represents the average from four samples in each diet group. For the hierarchical tree clustering of differentially expressed genes from liver, both genes and samples are clustered using Pearson dissimilarity.

SREBP1c activity

In order to ascertain whether an increase in key transcription factor SREP1c mRNA levels could result in an increase in hepatic SREBP1c activity, we used the Trans AM SREBP1c ELISA-based kit to determine SREBP1c activity in nuclear fractions of liver protein (**Fig. 4**) . An increase of 2.9-fold SREBP1c activity was seen in nuclear extracts from the TFA diet group compared with control. Specificity of SREBP1c binding is indicated by the fact that nuclear SREBP1 binding could be inhibited by a wild-type consensus oligonucleotide (Fig. 4; $P \leqslant 0.01$, n = 4).

Adipose tissue histology

Approximately 60% of hepatocellular lipid is derived from the circulation, particularly from adipose tissue stores (24). Since MSG diets markedly increased serum TG ($P = 0.0402$), FFA ($P \leqslant 0.0001$), and HDL-C levels ($P = 0.0022$) in our animal model, we next investigated visceral WAT distribution and histology in response to the four diets. **Figure 5A** shows increased abdominal WAT deposition in MSG, TFA, and TFA+MSG diet groups compared with control. Figure 5B shows micrographs of WAT stained with HE to demonstrate increase in adipocyte size in tissue from MSG, TFA, and TFA+MSG diet groups compared with control. Figure 5C shows quantitation of averaged adipocyte area. The largest increase in averaged WAT adipocyte size was seen in the TFA group, with up to 153.5 ±

TABLE 3. Diet-induced changes in hepatic gene expression. Microarray analysis of hepatic genes with ⩾1.5-fold changes in expression $P \leqslant 0.05$

Lipid Biosynthesis	Symbol	Accession	Control	MSG	TFA	TFA+MSG
Sterol regulatory element binding factor 1	Srebp1c	NM_011480	189.57	168.89	471.87	228.34
ATP citrate lyase	Acly	NM_134037	664.05	594.59	1051.89	655.50
Fatty acid synthase	Fasn	NM_007988	418.59	434.47	1005.81	545.56
Insulin-induced gene 1	Insig1	NM_153526	1579.06	1760.11	3266.25	1435.22
3-Hydroxy-3-methylglutaryl-CoA synthase 1	Hmgcs1	NM_145942	585.33	594.77	2088.10	672.34
3-Hydroxy-3-methylglutaryl-CoA synthase 2	Hmgcs2	NM_008256	9168.21	9217.89	7819.10	9021.49
Farnesyl diphosphate synthetase	Fdps	NM_134469	362.08	421.34	2438.01	750.66
Farnesyl diphosphate farnesyl transferase 1	Fdft1	NM_010191	469.36	510.99	1419.12	492.42
Farnesyl diphosphate synthetase	Fdps	NM_134469	362.08	421.34	2438.01	750.66
NAD(P)-dependent steroid dehydrogenase-like	Nsdhl	NM_010941	259.65	297.37	966.09	259.74
Phosphomevalonate kinase	Pmvk	NM_026784	105.56	107.04	327.52	167.62
Lanosterol synthase	Lss	NM_146006	119.99	140.68	299.70	154.20
Sterol-C5-desaturase (fungal ERG3, δ-5-desaturase)	Sc5d	NM_172769	2197.23	2223.47	3506.40	1911.46
Aldo-keto reductase family 1, member C6	Akr1c6	NM_030611	3125.29	3250.64	4752.36	3203.12
Stearoyl-CoA desaturase 2	Scd2	NM_009128	83.38	56.82	71.54	51.44
Elongation of very-long-chain fatty acids (FEN1)	Elovl1	NM_019422	379.07	393.05	494.06	405.41
NAD(P)-dependent steroid dehydrogenase-like	Nsdhl	NM_010941	259.65	297.37	966.09	259.74
Microsomal TG transfer protein	Mttp	NM_008642	2862.69	3058.72	1834.35	2141.64
Hydroxy-δ-5-steroid dehydrogenase, 3 β- and steroi	Hsd3b2	NM_153193	365.28	257.27	631.78	239.39
Hydroxy-δ-5-steroid dehydrogenase, 3 β- and ste	Hsd3b3	NM_001012306	1330.52	1023.44	2114.68	963.21
Progestin and adipoQ receptor family member VII	Paqr7	NM_027995	159.19	182.13	190.00	353.72
Progestin and adipoQ receptor family member III	Paqr3	NM_198422	155.50	158.90	96.77	216.84
Cubilin (intrinsic factor-cobalamin receptor)	Cubn	NM_001081084	28.50	25.15	21.41	36.78
Lipid Catabolism						
Peroxisomal trans-2-enoyl-CoA reductase	Pecr	NM_023523	815.22	783.62	1664.22	1376.71
Cytochrome b5 reductase 3	Cyb5r3	NM_029787	1694.74	1581.68	1744.30	1181.11
Cytochrome P450, family 2, subfamily b, polypeptide 9	Cyp2b9	NM_010000	17.91	78.97	131.30	120.23
Cytochrome P450, family 2, subfamily b, polypeptide 10	Cyp2b10	NM_009999	108.88	552.91	758.56	609.34
Cytochrome P450, family 2, subfamily c, polypeptide 55	Cyp2c55	NM_028089	70.61	162.96	245.09	60.60
Cytochrome P450, family 2, subfamily c, polypeptide 70	Cyp2c70	NM_145499	1254.49	1223.52	3494.99	795.21
Acyl-CoA dehydrogenase, medium chain	Acadm	NM_007382	4716.47	4713.76	4381.88	5645.38
Dodecenoyl-CoA δ isomerase (3,2 *trans*-enoyl-Coeny)	Dci	NM_010023	1526.43	1479.25	1485.38	1968.10
Flavin-containing monooxygenase 2	Fmo2	NM_018881	288.32	656.56	197.34	434.59
Phosphomevalonate kinase	Pmvk	NM_026784	105.56	107.04	327.52	167.62
Polyamine oxidase (exo-N4-amino)	Paox	NM_153783	264.73	261.92	473.21	335.55
Solute carrier family 25 (mitochondrial carrier)	Slc25a17	NM_011399	389.03	404.77	595.65	451.78
Carnitine acetyltransferase	Crat	NM_007760	1502.95	1668.15	839.21	1482.10
Lipid Transport and Storage						
ATP binding cassette, subfamily A (ABC1), member 8a	Abca8a	NM_153145	860.08	447.69	770.90	512.91
Cell death-inducing DNA fragmentation factor, α-subunit	Cidea	NM_007702	33.77	38.64	37.68	64.58
Cell death-inducing DFFA-like effector c	Cidec	NM_178373	253.58	479.34	225.48	1014.82
Adipose differentiation-related protein	Adfp	NM_007408	5098.92	5029.96	4313.63	6932.08
Prosaposin	Psap	NM_011179	5625.09	5467.62	4662.46	4887.37
Hexosaminidase A	Hexa	NM_010421	560.84	529.08	585.62	706.40
Phosphatidylinositol binding clathrin assembly protein	Picalm	NM_146194	1778.96	1908.01	1253.52	1640.35

TABLE 3. *Continued.*

Bile Acid Synthesis and Cholesterol Metabolism	Symbol	Accession	Control	MSG	TFA	TFA+MSG
Cytochrome P450, family 7, subfamily a, polypeptide 1	Cyp7a1	NM_007824	758.48	1911.92	939.67	1037.44
Nuclear receptor subfamily 0, group B, member 2 (SHP)	Nr0b2	NM_011850	744.96	406.88	777.83	304.72
Transcriptional Regulation						
Sterol regulatory element binding factor 1	Srebp1c	NM_011480	189.57	168.89	471.87	228.34
Growth arrest and DNA damage-inducible 45 β	Gadd45b	NM_008655	282.54	773.13	225.31	370.90
Aryl-hydrocarbon receptor	Ahr	NM_013464	541.77	852.06	551.65	455.79
NIPA-like domain containing 1	Npal1	NM_001081205	110.93	250.17	45.37	80.96
Insulin-induced gene 1	Insig1	NM_153526	1579.06	1760.11	3266.25	1435.22
Nuclear receptor subfamily 0, group B, member 2 (SHP)	Nr0b2	NM_011850	744.96	406.88	777.83	304.72
Nuclear factor, interleukin 3, regulated	Nfil3	NM_017373	265.94	468.14	422.16	368.93
Cell Cycle and Apoptosis						
P21 cyclin-dependent kinase inhibitor 1A	Cdkn1a	NM_007669	252.02	272.52	239.39	604.20
Growth arrest and DNA damage-inducible 45 β	Gadd45b	NM_008655	282.54	773.13	225.31	370.90
Centrin 2	Cetn2	NM_019405	35.67	35.40	86.04	51.60
Bcl2-associated athanogene 3	Bag3	NM_013863	514.97	618.01	374.13	615.89
BCL2-like 11 (apoptosis facilitator)	Bcl2l11	NM_207680	79.87	123.50	49.48	47.19
Inflammatory Response						
Interleukin 18	Il18	NM_008360	32.07	37.04	75.25	41.84
Interferon, α 14	Ifna14	NM_206975	75.74	45.85	54.05	103.42
Complement factor D (adipsin)	Cfd	NM_013459	54.48	52.69	109.46	407.39
Chemokine (C-C motif) ligand 2	Ccl2	NM_011333	34.75	27.59	34.73	46.66
Defensin β 1	Defb1	NM_007843	24.13	24.24	25.82	52.63
Torsin family 3, member A	Tor3a	NM_023141	134.19	157.66	88.71	224.31
Structural Constituent of Cytoskeleton						
Actin, γ, cytoplasmic 1	Actg1	NM_009609	1959.97	2341.08	2377.63	2877.08
Fibroblast growth factor 21	Fgf21	NM_020013	304.90	348.92	261.83	731.44
Annexin A2	Anxa2	NM_007585	54.34	63.53	102.36	78.08
Calsyntenin 3	Clstn3	NM_153508	60.32	69.81	72.62	135.77
Laminin, β 3	Lamb3	NM_008484	85.03	101.92	62.93	116.50
Ephrin A1	Efna1	NM_010107	276.99	457.27	373.05	209.17
Crystallin, γ B	Crygb	NM_144761	21.19	15.84	13.08	27.47
Cell Damage Marker						
Argininosuccinate lyase	Asl	NM_133768	5008.46	5930.57	3334.89	6084.01
Growth arrest and DNA damage-inducible 45 β	Gadd45b	NM_008655	282.54	773.13	225.31	370.90
Carbohydrate Metabolism						
Galactokinase 1	Galk1	NM_016905	237.64	296.28	378.86	507.36
Fructose bisphosphatase 2	Fbp2	NM_007994	46.92	40.65	45.40	60.00
Liver glycogen phosphorylase	Pygl	NM_133198	1474.25	1424.19	1960.87	1567.84
Glutathione Metabolism						
Isocitrate dehydrogenase 1 (NADP+), soluble	Idh1	NM_010497	2828.11	2901.25	4217.87	3364.13
Isocitrate dehydrogenase 2 (NADP+), mitochondrial	Idh2	NM_173011	674.66	736.07	885.77	984.01
Glutathione *S*-transferase, θ 3	Gstt3	NM_133994	335.28	576.31	497.21	377.23
Glutathione reductase 1	Gsr	NM_010344	1305.53	1541.80	1023.12	1083.99
Glutathione *S*-transferase, α 3	Gsta3	NM_001077353	4285.89	4668.83	6790.65	5407.37
Glutathione *S*-transferase, μ 2	Gstm2	NM_008183	288.04	417.56	318.20	271.85
Glutathione *S*-transferase, mu 3	Gstm3	NM_010359	551.31	985.96	864.76	403.68

TABLE 3. *Continued.*

Unknown	Symbol	Accession	Control	MSG	TFA	TFA+MSG
RIKEN cDNA A230097K15 gene	A230097K15Rik	NM_172715	129.36	127.69	146.97	344.17
Similar to Odc1 protein	LOC627245	XR_034503	90.99	93.91	98.45	187.99
Gene model 129, (NCBI) (Gm129), mRNA	Gm129	ENSMUST00000036418	63.49	76.90	59.84	114.15

Diet-induced changes in 16-week liver gene expression, according to function. Affymetrix analysis comparison within the four diet groups (control, MSG, TFA, and TFA+MSG). Only genes with significant changes in expression are listed (n = 4 per diet group; $P \leq 0.05$), with an arbitrary threshold of 1.5-fold.

5.1% increase compared with control cells. MSG increased adipocyte volume by up to 128.3 ± 7.0% of control. A comparable increase in adipocyte size was obtained in the TFA+MSG diet group (143.4 ± 5.1% of control, $P \leq 0.001$).

Adipose tissue gene expression

Affymetrix microarray analysis of visceral WAT genes with expression levels that were significantly different within the four diet groups is shown as a heat map with clustering dendogram in **Fig. 6** and numerically in **Table 4** ($P \leq 0.05$). A total of 169 genes were identified with significant differences in expression levels at a cutoff range of 1.5-fold. Unsurprisingly, the largest effect on WAT gene expression was obtained in animals fed the TFA diet, with increases in expression of lipogenic Stearoyl-CoA desaturase 2, Fasn, and Acly of 8.2-, 4.3-, and 4.2-fold compared with control. The MSG diet raised expression of several key lipid biosynthetic genes, including Fads2, the rate-limiting enzyme involved in mammalian synthesis of long-chain polyunsaturated fatty acids (25), and CDP-diacylglycerol synthase 1, a rate-limiting enzyme in the synthesis of phosphatidyl inositol (26). MSG also elevated the expression of WAT glycerol kinase and decreased levels of the energy-regulating mitochondrial carrier protein UCP3. Similarly, components of the mitochondrial reduction/oxidation reaction (REDOX) machinery, for example, Ndufs1, Ndufb4, and Ndufa10, were all upregulated in both TFA diet groups by 2.1-, 1.5-, and 1.8-fold, respectively. Interestingly, the expression of many WAT lipid catabolic proteins was decreased in MSG-treated animals, for example, short, medium, long, and very-long-chain acyl-CoA dehydrogenases (Acads, Acadm, Acadl, and Acadvl). REDOX-potentiating Lipin-1 gene expression was reduced in WAT tissue from both MSG diet groups (1.5- and 1.2-fold, respectively). The TFA diet had the opposite effect on the expression of these catabolic genes, with increases of 1.7-, 1.8-, 2.2-, and 2.1-fold, respectively.

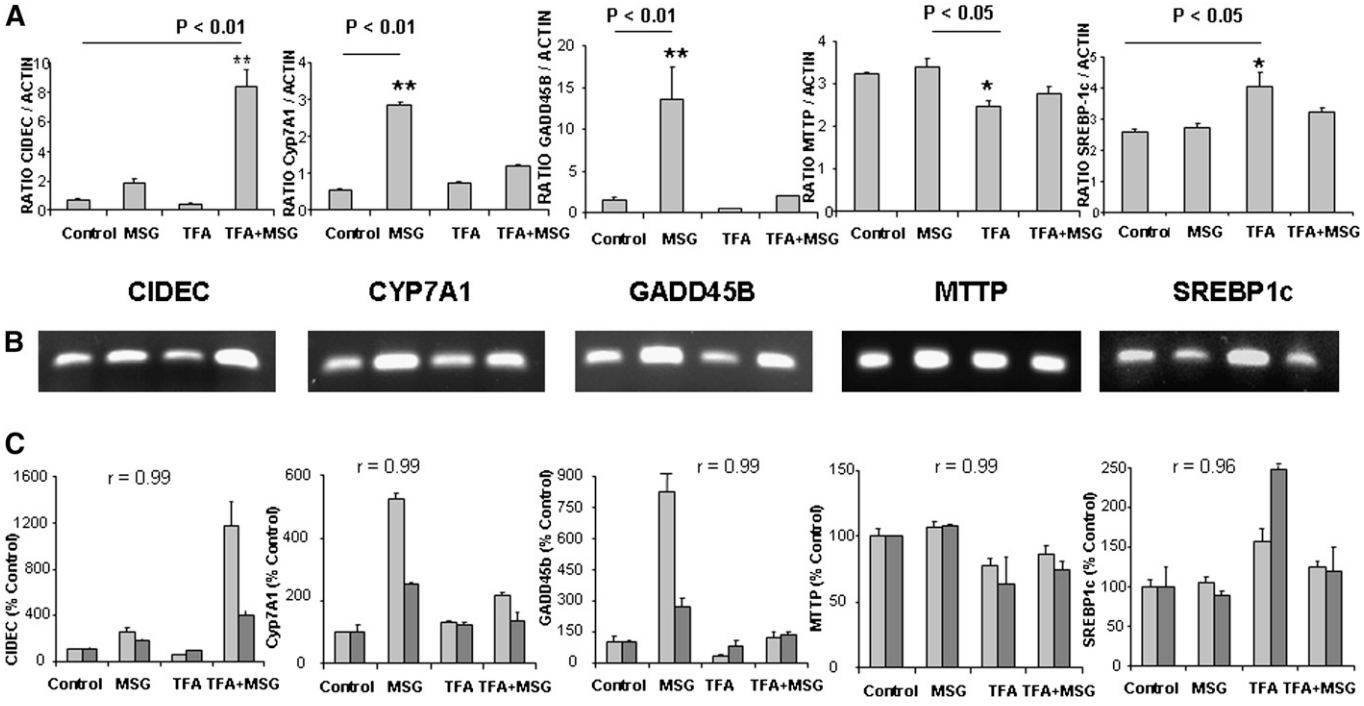

Fig. 3. Validation of Affymetrix microarray analysis of gene expression using qRT-PCR. A: qRT-PCR ratios of cyp7a1 (NM_ 007824), GADD45b (NM_008655), SREBP1c (NM_011480), CIDEC (NM_178373), and MTTP (NM_008642) relative to actin in 16-week-old mouse liver mRNA from the four different diet groups (control, MSG, TFA, and TFA+MSG; n = 4 per diet group). B: PCR products run on 2% agarose gel and stained with ethidium bromide. C: Concordance of qRT-PCR (light bars) versus microarray data (dark bars) for Cyp7a1, GADD45b, SREBP1c, CIDEC, and MTTP (signal intensity expressed as a percentage of control ± SD, n = 4 per diet group). Pearson correlation coefficients (r) are indicated for each bar chart. Results are representative of a minimum of two separate qRT-PCR experiments performed in triplicate.

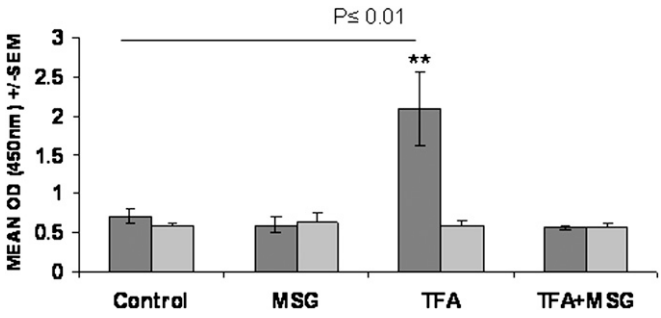

Fig. 4. Effect of diet on hepatic SREBP1c activity: SREBP1c DNA binding activity was determined using ELISA-based SREBP1c activation kit and quantified in triplicate by colorimetry. The levels of hepatic SREBP1c activity increased by 2.9-fold in the livers of TFA diet mice compared with control (dark gray bars, mean ± SEM, $P < 0.01$, n = 4 per diet group). Inclusion of a wild-type consensus oligonucleotide (light gray bars) attenuated the binding of nuclear SREBP1c, indicative of the specificity of the assay.

A combination of TFA+MSG lowered the expression of these and other TFA-induced catabolic genes, including hydroxyacyl-CoA dehydrogenase, enoyl CoA hydratase, and acyl-CoA synthase. Conversely, the expression of several lipogenic TFA-induced enzymes was significantly augmented by the addition of MSG, including Fatty acid desaturase 1 and Stearoyl-CoA desaturase 4. Transcriptional regulation of a number of genes affected by these diets are under the control of ligand-activated transcription factors, such as peroxisome proliferator-activated receptor-α (Pparα) and Pparδ. TFA induced the expression of PPARα by 1.8-fold; however, this increase was attenuated in the TFA+MSG diet. Expression of the key energy regulator Ppargc1a was reduced by half in WAT from MSG-treated animals. A similar reduction was seen in the TFA diet group, and expression of this key energy regulator was reduced to 25% in the TFA+MSG-treated animals, making this gene a likely candidate in regulating WAT adipocyte responses to these three diets. Conversely, levels of SREBP1c were increased in both TFS diets by approximately 3-fold.

Taken together, these results indicate that MSG increases the expression of a number of genes involved in de novo lipogenesis and adipocyte differentiation, while lowering the expression of lipid-catabolizing proteins in WAT tissue. TFA, on the other hand, enhances both lipogenic and lipid catabolic (oxidative) gene expression. A combination of TFA+MSG resulted in a decrease in lipid-catabolizing gene expression and an increase in several lipid biosynthetic genes, resulting in a net increase in serum TG and T-CHOL of 39.3% and 10.5%, respectively.

DISCUSSION

The incidence of NAFLD is increasing throughout the world (1, 2), and its etiology, though not fully understood,

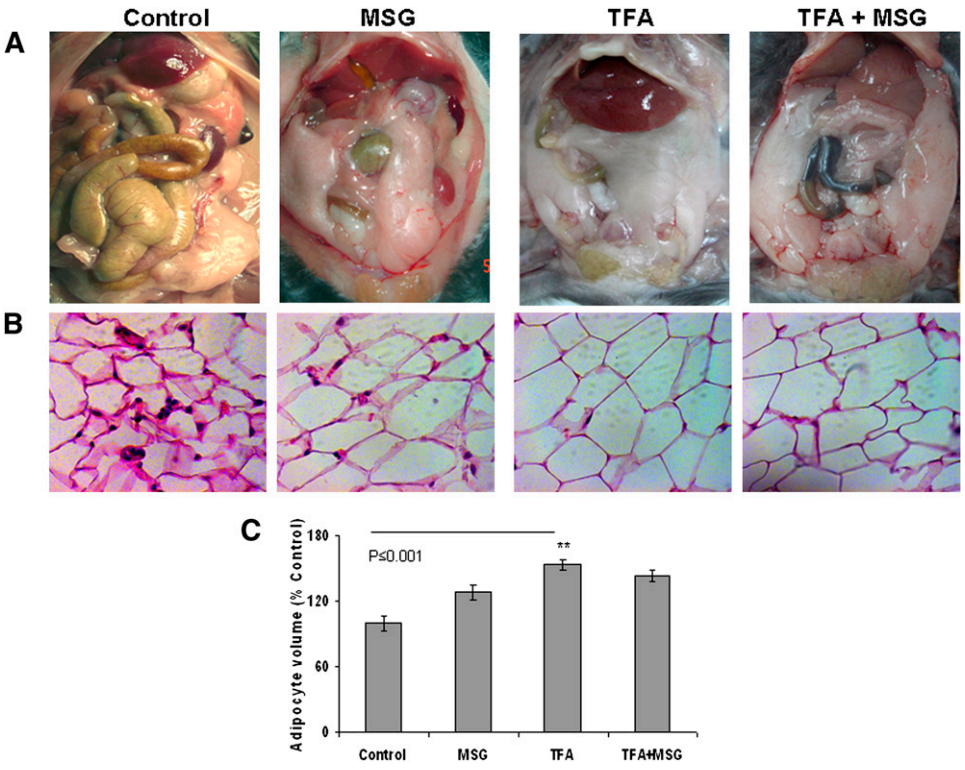

Fig. 5. Diet-induced changes in visceral fat histology. A: Increased abdominal adipose distribution in 32-week-old mice from MSG, TFA, and TFA+MSG diet groups compared with control. B: HE-stained micrograph depicting increased adipocyte volume in visceral adipose tissues from MSG, TFA, and TFA+MSG treated mice compared with control. Results are representative of four separate experiments. C: Quantitation of changes in adipocyte area. The data are expressed as the means ± SEM of at least 30 cells per diet group ($P \leq 0.001$).

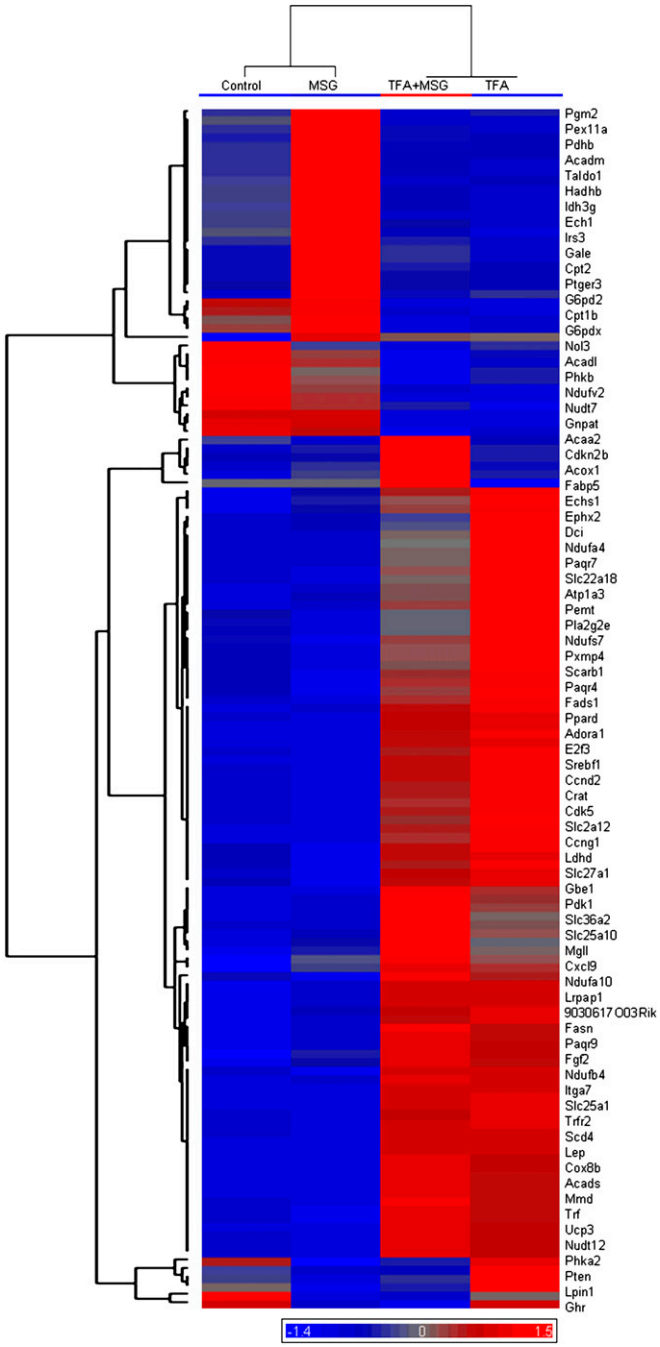

Fig. 6. WAT expression heat map and unsupervised hierarchical clustering analysis. Red pseudocolor and blue represents upregulated and downregulated genes, respectively. Each row represents a differentially expressed gene within livers from mice in the four diet groups ($P \leq 0.05$). Each column represents the average from four samples in each diet group. For the hierarchical tree clustering of differentially expressed genes from liver, both genes and samples are clustered using Pearson dissimilarity.

is believed to include dietary factors. Practically unheard of prior to the 1980s, NAFLD now affects approximately 15–25% of the general population (1); thus, the cause of this progressive disease is unlikely to be due to genetic abnormalities. Among the several major changes to the global diet during the past 35 years is the introduction of *trans*-hydrogenated dietary oils into the food chain. TFAs are formed by configurational isomerization of *cis*-fatty acids, which results in a prolonged shelf life of vegetable fats and any food products that contain them. However once ingested and incorporated, TFA affects tissue composition and functionality (27). TFA ingestion has been associated with cardiovascular complications and weight gain (28). Central obesity can also be induced experimentally by neonatal administration of the ubiquitous dietary flavor enhancer MSG, at a time when the blood-brain barrier is compromised (15). Hepatic dysplasia was also recently demonstrated following neonatal MSG administration (16); however, the mechanism remains largely unknown. In this article, we first examine the mechanism of TFA-induced NAFLD and the contribution of abdominal WAT lipogenesis to the liver pathology, in an animal model of diet-induced fatty liver disease. Second, we investigate whether dietary MSG could contribute to the pathology of NAFLD, either alone or in combination with TFA. A combination of 60% fat and/or neonatal administration of MSG was recently demonstrated to induce obesity in C57BL/6J and NMRI mice; however, the molecular mechanisms behind this were not fully addressed (14). An acceptable daily intake for MSG has been set at 0–120 mg/kg bw (17). The oral dose of MSG used in this study (91 mg/kg bw) reflects current consumption levels (18) and is 30–40 times less than the level previously reported to induce neuronal damage when injected neonatally (13–15). Because it has previously been suggested that MSG excitotoxicity occurs only when the blood-brain barrier is vulnerable, for example, neonatally (15), we studied C57Bl/6J mice that had been bred and weaned from animals maintained on the respective diets for a 3-week run-in period prior to mating. Interestingly, fasting leptin levels in mice from the MSG diet group were no different than controls. However, leptin levels were raised in the TFA diet and in the TFA+MSG diet group. Since it is known that neonatally injected MSG-lesioned mice with resultant arcuate nucleus ablation exhibit robust hyperleptinemia (14), one interpretation of our results suggests that the low-dose dietary MSG in our model was insufficient to completely impair MSG-sensitive areas of the brain.

Dyslipidemia was apparent in MSG, TFA, and TFA+MSG diet groups compared with control. In the absence of increased exogenous dietary lipid, MSG significantly elevated serum FFA, TG, and HDL-C, while reducing weight gain. TFA feeding increased weight gain, FFA, and HDL-C; however, the largest effect on lipid homeostasis was seen in the TFA+MSG diet, which resulted in a 40% increase in TG levels together with a 10% increase in T-CHOL. Hepatic steatosis with necroinflammatory changes was recently observed in mice fed a diet containing 45% of calories derived from fat, together with a high-fructose corn syrup equivalent of 42 g/l (29). In this model, 30% of the dietary fat was in the form of partially hydrogenated vegetable oil, and interestingly when this was replaced by isocaloric amounts of lard, the extent of steatosis was substantially reduced, indicating greater liver injury with the consumption of synthetic TFA (29).

TABLE 4. Diet-induced changes in WAT gene expression: microarray analysis of WAT genes with ⩾1.5-fold changes in expression $P \leqslant 0.05$

Adipocyte Regulation	Symbol	Accession Number	Control	MSG	TFA	TFA+MSG
Peroxisome proliferative activated receptor γ, coa	Ppargc1a	NM_008904	207.785	100.571	98.2685	53.8478
Peroxisome proliferator activated receptor α	Ppara	NM_011144	93.0644	97.1972	170.085	109.412
Peroxisome proliferator activator receptor delta	Ppard	NM_011145	294.718	259.436	349.966	386.123
Sterol regulatory element binding factor 1	Srebp1c	NM_011480	274.904	365.423	814.998	804.859
Phosphatase and tensin homolog	Pten	NM_008960	2403.1	1910.83	2924.98	2165.36
Uncoupling protein 3 (mitochondrial, proton carrier)	Ucp3	NM_009464	350.936	243.233	386.359	298.198
Leptin	Lep	NM_008493	416.213	307.025	752.926	858.808
Lipin 1	Lpin1	NM_015763	3840.64	2586.07	3144.98	2671.4
Lipid Biosynthesis						
ATP citrate lyase	Acly	NM_134037	569.674	721.338	2404.7	1598.01
Fatty acid synthase	Fasn	NM_007988	1427.5	1097.72	6193.61	6135.52
Stearoyl-CoA desaturase 2	Scd2	NM_009128	248.052	743.632	2026.87	1376.59
Stearoyl-CoA desaturase 4	Scd4	NM_183216	195.18	174.295	288.325	317.439
Fatty acid desaturase 1	Fads1	NM_146094	532.43	1033.2	1297.99	1565.13
Fatty acid desaturase 2	Fads2	NM_019699	249.105	1125.61	393.17	307.361
CDP-diacylglycerol synthase 1	Cds1	NM_173370	89.3485	261.925	86.8198	97.0006
Glycerol kinase	Gyk	NM_212444	123.172	324.475	80.2213	67.8314
Monoglyceride lipase	Mgll	NM_011844	1970.21	2008.02	3234.97	3129.91
Solute carrier family 27 (fatty acid transporter)	Fatp	NM_011977	4126.25	4876.71	6112.56	6533.57
Solute carrier family 25 (mitochondrial carrier, citrate)	Slc25a1	NM_153150	799.205	835.45	3776.75	4510.9
Solute carrier family 25 (mitochondrial carrier, dicarb)	Slc25a10	NM_013770	213.472	270.111	1441.15	1375.56
Sortilin-related receptor, LDLR class A repeat-containing	Sorl1	NM_011436	140.952	221.001	403.261	332.49
Lipid Catabolism						
Phospholipase A2, group IIE	Pla2g2e	NM_012044	69.5803	71.8988	234.393	409.934
Acyl-CoA dehydrogenase, short chain	Acads	NM_007383	591.962	528.448	986.071	1061.57
Acyl-CoA dehydrogenase, medium chain	Acadm	NM_007382	3153.68	2620.15	5509.32	4119.16
Acyl-CoA dehydrogenase, long-chain	Acadl	NM_007381	1473.38	1264.05	3219.5	2764.69
Acyl-CoA dehydrogenase, very long chain	Acadvl	NM_017366	612.052	451.538	1311.61	817.799
Acyl-CoA synthetase long-chain family member 3	Acsl3	NM_028817	136.342	122.228	390.947	261.356
Acetyl-CoA acyltransferase 2 (mitochondrial 3-oxoacetate)	Acaa2	NM_177470	936.529	883.846	1555.85	1297.6
Acyl-CoA oxidase 1, palmitoyl	Acox1	NM_015729	3636.48	3615.39	5548.38	4840.69
Enoyl-CoA, hydratase	Ehhadh	NM_023737	646.783	631.701	1921.61	1152.28
Enoyl CoA hydratase, short chain 1, mitochondrial	Echs1	NM_053119	1223.48	1034.78	1843.09	1676.75
Carnitine palmitoyltransferase 1b, muscle	Cpt1b	NM_009948	33.2879	30.2366	97.4969	78.2812
Carnitine palmitoyltransferase 2	Cpt2	NM_009949	461.32	428.067	1039.18	931.86
Sortilin-related receptor, LDLR class A repeat-containing	Sorl1	NM_011436	140.952	221.001	403.261	332.49
Carnitine acetyltransferase	Crat	NM_007760	1516.47	1753.05	2725.49	2528.82
Fatty acid binding protein 5, epidermal	Fabp5	BC002008	477.11	325.212	1062.18	889.972
Hydroxyacyl-CoA dehydrogenase	Hadhb	NM_145558	1635.31	1284.78	2899.93	2340
Hydroxysteroid 11-β dehydrogenase 1	Hsd11b1	NM_008288	778.484	744.313	303.153	295.215
Pyruvate dehydrogenase kinase, isoenzyme 1	Pdk1	NM_172665	191.081	208.573	399.007	413.604
Pyruvate dehydrogenase complex, component X	Pdhx	NM_175094	199.948	140.753	409.825	255.335
Pyruvate dehydrogenase (lipoamide) β	Pdhb	NM_024221	1065.04	894.9	1901.62	1446.57
Dodecenoyl-CoA δ isomerase	Dci	NM_010023	1136.22	992.017	1688.27	1604.81
Apolipoprotein D	APOD	NM_007470	501.426	710.941	233.76	194.34
NADH dehydrogenase (ubiquinone) Fe-S protein 1	Ndufs1	NM_145518	828.715	727.273	1762.18	1183.79
NADH dehydrogenase (ubiquinone) 1 α subcomplex, 4	Ndufa4	NM_010886	3020.26	2629.76	4249.85	3995.4
NADH dehydrogenase (ubiquinone) 1 β subcomplex 4	Ndufb4	NM_026610	844.531	850.11	1271.31	1367.65
NADH dehydrogenase (ubiquinone) Fe-S protein 7	Ndufs7	NM_029272	992.445	1153	1499.14	1940.24
NADH dehydrogenase (ubiquinone) 1 α subcomplex 10	Ndufa10	NM_024197	1181.01	1101.3	2140.55	2047.87
NADH dehydrogenase (ubiquinone) flavoprotein 2	Ndufv2	NM_028388	817.676	779.237	1138.18	1032.68
Isocitrate dehydrogenase 3 (NAD+), γ	Idh3g	NM_008323	1810.56	1625.33	2679.26	2273.07
Cytochrome b5 type B	Cyb5b	NM_025558	525.932	690.39	1697.57	1111.23
Nucleolar protein 3 (apoptosis repressor with CARD domain)	Nol3	NM_030152	168.191	133.963	576.919	474.77
Lactate dehydrogenase D	Ldhd	NM_027570	131.619	256.175	432.356	463.235
Cytochrome b5 type B	Cyb5b	NM_025558	525.932	690.39	1697.57	1111.23
Desmoplakin	Dsp	XM_621314	82.066	183.205	39.4581	38.2632
Arginase type II	Arg2	NM_009705	56.1506	140.53	24.8147	40.5973
Cytochrome c oxidase, subunit VIIIb	Cox8b	NM_007751	54.2939	36.4708	323.583	362.081

TABLE 4. *Continued.*

Peroxisomal Function	Symbol	Accession Number	Control	MSG	TFA	TFA+MSG
Isopentenyl-diphosphate δ isomerase	Idi1	NM_177960	149.455	172.681	537.381	302.674
Enoyl-CoA, hydratase	Ehhadh	NM_023737	646.783	631.701	1921.61	1152.28
Peroxisomal biogenesis factor 11a	Pex11a	NM_011068	392.622	336.662	721.9	542.704
Peroxisomal δ3, δ2-enoyl-CoA isomerase	Peci	NM_011868	732.736	666.183	1187.13	860.848
Peroxisomal membrane protein 4	Pxmp4	NM_021534	605.243	676.353	751.33	977.305
Epoxide hydrolase 2, cytoplasmic	Ephx2	NM_007940	2437.66	2024.21	3942.09	3416.06
Nudix (nucleoside diphosphate linked moiety X)-type motif	Nudt7	NM_024437	346.175	299.425	938.568	724.774
Nudix (nucleoside diphosphate linked moiety X)-type motif	Nudt12	NM_026497	361.798	316.533	547.101	324.397
Glyceronephosphate *O*-acyltransferase	Gnpat	NM_010322	1096.27	1032.77	2105.46	1774.53
Signal Transduction						
Prostaglandin E receptor 3 (subtype EP3)	Ptger3	NM_011196	117.946	99.421	1187.98	922.455
Adrenergic receptor, α 1a	Adra1a	NM_013461	45.6034	52.3072	141.729	92.2266
Adenosine A1 receptor	Adora1	NM_001008533	158.242	209.451	401.644	407.347
Insulin receptor substrate 3	Irs3	NM_010571	155.999	167.76	370.544	320.495
Fibroblast growth factor 2	Fgf2	NM_008006	122.023	128.377	276.782	310.22
Pyruvate dehydrogenase kinase, isoenzyme 1	Pdk1	NM_172665	191.081	208.573	399.007	413.604
Transport						
Solute carrier family 25 (mitochondrial carrier, dicarboxylate)	Slc25a10	NM_013770	213.472	270.111	1441.15	1375.56
Solute carrier family 25 (mitochondrial carrier, citrate)	Slc22a1	NM_153150	799.205	835.45	3776.75	4510.9
Solute carrier family 44	Slc44a2	NM_153170	779.389	773.121	2970.71	3067.1
LDL receptor	ldlr	NM_010700	72.247	79.8331	233.701	140.419
ATPase, Na^+	Atp1a3	NM_144921	75.3448	77.6205	193.636	278.764
Solute carrier family 22 (organic cation transporter)	Slc22a18	NM_001042760	68.634	71.2359	160.196	219.99
Solute carrier family 2 (facilitated glucose transporter)	Slc2a12	NM_178934	120.203	139.598	200.664	216.288
Solute carrier family 2 (facilitated glucose transporter)	sSlc2a8	NM_019488	142.751	147.964	151.067	221.085
Receptors						
Peroxisome proliferator activated receptor α	Ppara	NM_011144	93.0644	97.1972	170.085	109.412
Peroxisome proliferator activator receptor δ	Ppard	NM_011145	294.718	259.436	349.966	386.123
Prostaglandin E receptor 3 (subtype EP3)	Ptger3	NM_011196	117.946	99.421	1187.98	922.455
Progestin and adipoQ receptor family member IX	Paqr9	NM_198414	79.6942	92.1643	298.852	333.561
Progestin and adipoQ receptor family member VII	Paqr7	NM_027995	50.2071	51.0594	80.4598	98.048
Progestin and adipoQ receptor family member IV	Paqr4	NM_023824	68.3874	97.996	107.27	128.582
LDL receptor	Ldlr	NM_010700	72.247	79.8331	233.701	140.419
LDL receptor-related protein associated	Lrpap1	NM_013587	756.137	643.336	1588.01	1567.44
v-erb-b2 erythroblastic leukemia viral oncogene homolog 3	Erbb3	NM_010153	52.7788	197.737	28.0029	28.6486
Adrenergic receptor, α 1a	Adra1a	NM_013461	45.6034	52.3072	141.729	92.2266
G protein-coupled receptor, family C, group 5, member C	Gprc5c	NM_147217	93.3337	203.394	89.2327	95.972
Thyroid stimulating hormone receptor	Tshr	NM_011648	816.095	812.633	1270.21	1012.98
Scavenger receptor class B, member 1	Scarb1	NM_016741	569.797	770.378	945.168	1354.36
Insulin receptor substrate 3	Irs3	NM_010571	155.999	167.76	370.544	320.495
Insulin receptor substrate 1	Irs1	NM_010570	416.333	437.413	351.945	291.675
Insulin-like growth factor I receptor	Igf1r	NM_010513	178.257	251.664	119.552	101.203
Transferrin receptor	Tfrc	NM_011638	122.905	144.103	410.862	213.467
Transferrin receptor 2	Trfr2	NM_015799	24.9875	21.8008	46.393	54.1345
Fibroblast growth factor receptor 2	Fgfr2	NM_010207	99.2272	176.365	97.9843	78.6453
LDL receptor-related protein associat	Lrpap1	NM_013587	756.137	643.336	1588.01	1567.44
Inositol 1,4,5-triphosphate receptor 3	Itpr3	NM_080553	102.899	158.906	84.5433	88.4972
Epidermal growth factor receptor	Egfr	NM_207655	638.061	590.145	420.657	372.95
Platelet derived growth factor receptor, α polypeptid	Pdgfra	NM_011058	704.318	538.599	431.001	302.329
CD80 antigen (Cd80), mRNA	Cd80	ENSMUST0 0000099816	61.8466	49.2382	35.9132	28.2798
CD86 antigen	Cd86	NM_019388	103.315	84.6118	58.7097	50.05
Plasminogen activator, urokinase receptor	Plaur	NM_011113	154.832	120.529	71.7527	80.9476
KDEL (Lys-Asp-Glu-Leu) endoplasmic reticulum protein rete	Kdelr3	NM_134090	62.1696	70.3587	35.8343	33.9707
Interleukin 1 receptor-like 2	Il1rl2	NM_133193	114.778	81.3391	65.5971	47.7045
Growth hormone receptor	Ghr	NM_010284	4786.35	4049.57	4771.72	3858.85

TABLE 4. *Continued.*

Adipocyte Differentiation	Symbol	Accession Number	Control	MSG	TFA	TFA+MSG
Fibroblast growth factor receptor 2	Fgfr2	NM_010207	99.2272	176.365	97.9843	78.6453
Integrin α 7	Itga7	NM_008398	276.428	278.804	590.437	672.718
Cadherin 1	Cdh1	NM_009864	68.6827	232.39	52.9224	56.5541
Transmembrane protease, serine 2	Tmprss2	NM_015775	39.573	103.104	21.2998	24.7111
Fibromodulin	Fmod	NM_021355	205.372	348.217	169.39	198.026
Fibroblast growth factor 8	Fgf8	NM_010205	78.4366	67.4992	70.6433	119.504
Fibroblast growth factor 11	Fgf11	NM_010198	50.8896	53.448	53.9365	75.8426
Transferrin	Trf	NM_133977	8064.93	7765.66	9918.24	10155.1
Monocyte to macrophage differentiation-associated	Mmd	NM_026178	2283.47	2097.05	3941.05	4259.07
Cell Cycle and Apoptosis						
Cyclin G1	Ccng1	NM_009831	1229.2	1446.48	2290.95	2461.64
Cyclin D2	Ccnd2	NM_009829	1396.37	1656.5	2387.41	2270.71
Cyclin-dependent kinase 5	Cdk5	NM_007668	252.7	285.747	411.265	457.847
Cyclin-dependent kinase inhibitor 2B (p15, inhibits CDK4)	Cdkn2b	NM_007670	83.8559	85.6237	166.889	141.524
Cyclin-dependent kinase inhibitor 1C (P57)	Cdkn1c	NM_009876	457.521	457.465	241.507	256.232
Cyclin-dependent kinase inhibitor 1A (P21)	Cdkn1a	NM_007669	696.342	564.085	271.24	407.371
E2F transcription factor 3	E2f3	NM_010093	61.8946	69.2646	108.639	107.949
Growth hormone receptor	Ghr	NM_010284	4786.35	4049.57	4771.72	3858.85
Fas apoptotic inhibitory molecule 2	Faim2	NM_028224	36.9562	80.198	34.7032	41.1719
Sphingosine-1-phosphate phosphatase 1	Sgpp1	NM_030750	354.925	828.114	314.766	397.005
Detoxification						
Glutathione *S*-transferase, μ 7	Gstm7	NM_026672	362.098	1364.96	301.501	369.097
Transporter Activity						
Adaptor protein complex AP-1, μ 2 subunit	Ap1m2	NM_009678	47.9936	121.543	36.5898	40.1935
Solute carrier family 24 (sodium)	Slc24a6	NM_133221	347.873	349.597	263.234	436.4
Solute carrier family 38, member 4	Slc4a4	NM_027052	53.6172	204.553	19.4335	25.3937
Phosphatidylethanolamine *N*-methyltransferase	Pemt	NM_008819	88.1222	99.0729	153.149	246.455
Potassium inwardly-rectifying channel, subfamily J, membe	Kcnj16	NM_010604	39.0206	172.841	15.6521	19.4124
Potassium channel, subfamily K, member 1	Kcnk1	NM_008430	153.771	676.244	49.1542	58.9303
G protein-coupled receptor, family C, group 5, member C	Gprc5c	NM_147217	93.3337	203.394	89.2327	95.972
Ubiquitin-specific peptidase 54	Usp54	NM_030180	323.957	244.033	103.714	98.8471
Carbohydrate Metabolism						
Glucose-6-phosphate dehydrogenase X-linked	G6pdx	NM_008062	1481.98	1379.61	3714.84	3113.7
Glucose-6-phosphate dehydrogenase 2	G6pd2	NM_019468	669.507	662.022	1602.29	1400.55
Phosphorylase kinase β	Phkb	NM_199446	394.127	354.805	796.981	675.093
Galactose-4-epimerase, UDP	Gale	NM_178389	95.505	89.5107	190.082	172.788
Carbohydrate kinase-like	Carkl	NM_029031	69.8275	84.668	114.601	96.5293
Transaldolase 1	Taldo1	NM_011528	963.615	799.463	1574.04	1289.01
Phosphoglucomutase 2	Pgm2	NM_028132	1156.14	951.663	1800.34	1449.66
Glucan (1,4-α-), branching enzyme 1	Gbe1	NM_028803	689.557	584.177	1069.62	1086.39
Galactosidase, β 1	Glb1	NM_009752	196.664	281.974	250.851	251.99
Phosphorylase kinase α 2	Phka2	NM_172783	560.735	498.458	677.721	548.902
Carbohydrate (keratan sulfate Gal-6) sulfotransferase 1	Chst1	NM_023850	408.016	534.732	484.569	823.109
Solute carrier family 2 (facilitated glucose transporter)	Slc2a1	NM_011400	328.917	391.346	166.779	193.015
Inflammatory Response						
Chemokine (C-X-C motif) ligand 9	Cxcl9	NM_008599	362.594	320.708	644.394	612.101
Carbohydrate (keratan sulfate Gal-6) sulfotransferase 1	Chst1	NM_023850	408.016	534.732	484.569	823.109
Unknown Function						
RIKEN cDNA 2010100O12 gene	2010100O12Rik	BC028749	641.873	701.625	671.019	1011.38
RIKEN cDNA 9030617O03 gene	030617O03Rik	BC066161	80.5232	75.9806	178.859	174.893

Visceral adipose tissue Affymetrix microarray analysis of gene expression: list of genes with significantly different expression changes ($P \leq 0.05$) within the four diet groups (control, MSG, TFA, and TFA+MSG) with an arbitrary threshold of 1.5-fold.

Hepatic steatosis and gene expression

Increased hepatic TG content and microsteatosis were apparent in MSG-treated animals, in agreement with previous observations by Nakanishi et al. (16). The liver weight, a marker of steatohepatitis (30), increased by up to 1.5-fold in TFA+MSG-treated animals. We used Affymetrix microarray to investigate the possible mechanisms for the MSG-induced hepatic dyslipidemia. Most notably, we found that the expression of hepatic genes involved in β-oxidation of fatty acids, bile acid synthesis, and lipid storage was upregulated in MSG-treated mice. Expression of steroid hydroxylases Cyp2b9 and Cyp2b10 was elevated by MSG treatment, together with an increase in Cyp2c55, implicated in AA and linoleic acid catabolism. Evidence for enhanced fatty acid oxidation in NAFLD is provided by Kohjima et al. (31), who found elevated expression of oxidation-related Cyp2E1 and Cyp4A11 genes among others. In our study, increased microsomal oxidative Fmo2 expression by MSG treatment was accompanied by an elevation in the transcription factor Ahr, believed to modulate the expression of numerous genes involved in cholesterol biosynthesis and fatty acid synthesis (32). Initially, research focused on the role of Ahr in the induction of AA-epoxygenative Cyp1 (33); however, it is now thought that Ahr plays a more comprehensive role in lipid homeostasis via downregulation of the nuclear receptor Pparα (34). In addition to metabolizing endogenous and exogenously derived lipids, circulating cholesterol is taken up and metabolized in the liver. Dietary MSG elevated serum HDL-C and increased the expression of Cyp7a1, a key regulatory protein in the classical pathway of bile acid formation (22), while lowering the expression of the nuclear receptor SHP, which has been found to negatively regulate FXR-dependent inhibition of Cyp7a1 transcription. In NAFLD, only roughly one-quarter of hepatic TG is formed from de novo biosynthesis, the rest being derived from dietary sources and uptake of serum FFA (35). Excess circulating lipids can be taken up and stored in hepatic lipid droplets (23), and Fat-Specific Protein 27 (CIDEC) is one of the main proteins implicated in this process. In our study, hepatic lipid deposition was accompanied by an increase in CIDEC expression, occurring in both the MSG and the TFA+MSG diet groups. Taken together, these results suggest that MSG diets elevate serum lipids and activate genes involved in the storage, oxidation, and clearance of exogenous lipids via activation of the bile acid pathway.

Genes involved in de novo lipogenesis and cholesterol synthesis, such as Acly, FAS, and Hsd3b3, were downregulated in MSG-treated animals. Conversely, these and many other genes were upregulated by *trans*-fat feeding, including the transcriptional regulatory element SREBP1c. NAFLD patients have higher levels of SREBP1c and lipogenic gene expression, believed to be the result of impaired insulin signaling (36). Elevated SREBP1c, Acly, FAS, and other genes involved in the de novo synthesis and uptake of fatty acids have been reported in animal models of NAFLD (37) as well as human studies (36). SREBP1c is synthesized as an inactive precursor protein bound to the endoplasmic reticulum and nuclear envelope. Once activated by sterol deprivation, the precursor protein is cleaved to release the activated N-terminal portion, which then enters the nucleus and activates transcription of genes involved in cholesterol and fatty acid synthesis. We used an ELISA-based colorimetric Trans AM SREBP1c assay to confirm that TFA-induced increases in SREBP1c mRNA lead to an increase in SREBP1c activity, in nuclear extracts of the livers of mice from the TFA diet groups.

Accompanying the increased de novo lipogenesis, livers of TFA+MSG-fed mice had evidence of an increased inflammatory response, with elevated adipsin expression (complement Factor D). Adipsin is the rate-limiting step in the alternative complement pathway and is activated in alcoholic fatty liver disease (38). Interferon-α14, and defensin β1, part of the innate immune response (39), were also increased. Additionally, livers of TFA+MSG-treated animals had upregulated levels of Fibroblast Growth Factor 21, laminin, and actin-γ, together with raised p21 levels. Inflammation and fibrosis are hallmarks of NASH, the severity of each correlating well with levels of hepatic bile acids in these patients (40). Expression of p21, a universal inhibitor of cyclin-dependent kinases and replicative arrest, was markedly increased in TFA+MSG-treated livers. P21 overexpression is associated with enlarged nuclei (41) and was also present in the livers of mice in this diet group. Elevated p21 has previously been shown to correlate with periportal fibrogenesis in patients with NASH (42).Taken in composite, these results suggest that in the absence of high dietary fat, MSG induces the expression of lipid oxidizing and storage genes. TFA, however, induces genes involved in de novo lipid synthesis as well as catabolism. The addition of MSG to the TFA diet appeared to decrease the expression of genes associated with hepatic de novo lipid synthesis, while increasing fat storage genes, inflammatory markers, profibrogenic markers, and p21 associated with replicative arrest.

Contribution of adipose tissue to diet-induced NAFLD

We next examined the contribution of diet-induced WAT gene expression to the pathology of NAFLD because it has recently been shown that visceral fat is an independent predictor of advanced steatohepatitis (43). Visceral adiposity and adipocyte size were increased in all three diet groups compared with control. Adipocyte size has recently been shown to correlate well with regional fat mass by Tchoukalova et al. (44). In WAT, expression of key regulatory protein Ppargc1a was halved by MSG or TFA-containing diets and quartered by a combination of TFA+MSG. Expression of Ppargc1a is reduced in obesity, and this is accompanied by decreased mitochondrial fatty acid oxidation due to coordinated downregulation of genes involved in this pathway (45). Additionally, genetic polymorphisms in Ppargc1a resulting in liver levels of Ppargc1a mRNA have been observed in patients with NAFLD (46). In our study, MSG reduced the expression of several WAT β-oxidative genes, whereas TFA markedly enhanced their expression. Unsurprisingly, Pparα and Pparδ levels were

enhanced in the TFA diet group, as it has previously been demonstrated that these nuclear receptors regulate fatty acid degradation (47, 48). Conversely, Pparα and Pparδ levels were unchanged in the MSG diet groups, and Lipin-1, an inducible amplifier of mitochondrial oxidation (49), was significantly reduced. Lipin-1 can be induced by Ppargc1a and is believed to activate Pparα target pathways to increase lipid catabolism (49). Reduced Lipin-1 activity is also seen in obesity (50), adding support to the notion that dietary MSG may decrease adipocyte fatty acid oxidation. Several key WAT lipogenic genes were upregulated in MSG-treated animals, including FADS2, the rate-limiting enzyme involved in mammalian synthesis of long-chain polyunsaturated fatty acids (25), CDP-diacylglycerol synthase 1, a rate-limiting enzyme in the synthesis of phosphatidyl inositol (26), and glycerol kinase. MSG-induced enhancement of the expression of these enzymes may account for the marked elevation in serum FFA and TG observed in this study.

The *trans*-fat diet induced WAT expression of many lipogenic proteins, including Acly, FAS, and Stearoyl-CoA desaturase 2. SREBP1c, known to regulate lipogenic gene expression (51), was also elevated in this diet group, together with increased leptin and LDL receptor levels, indicative of an obesogenic expression profile.

The highest levels of serum T-CHOL and HDL-C were seen in the TFA+MSG diet group. Adipocytes are capable of de novo TG and cholesterol synthesis and storage (52), with adipocyte size correlating well with cholesterol and TG content. We looked for WAT genes in the TFA+MSG diet group with the highest change in expression that might account for the accompanying elevation in serum lipids. Expression of Fatty acid desaturase 1, Stearoyl-CoA desaturase 4, Phospholipase A2, scavenger receptor-B1, and Fatty Acid Transporter were all highest in this group, suggesting that genes involved in lipogenesis and fat storage were upregulated. Additionally, genes involved in adipocyte differentiation, including leptin, Fgf-8, Fgf-11, and monocyte to macrophage differentiation-associated protein, were maximally elevated in the TFA+MSG diet group relative to the other groups.

In conclusion, we have established an animal model of diet-induced NAFLD that has allowed us to speculate on the contribution of abdominal WAT to the pathogenesis of hepatic steatosis. Dietary MSG at doses similar to the average daily intake caused hepatic microsteatosis and the expression of β-oxidative genes in the offspring of mice previously established on the diet. Fasting serum TG, FFA, and insulin levels were elevated. WAT adipocytes were enlarged and showed an increase in lipid biosynthetic gene expression and a decrease in Ppargc1a levels. *Trans*-fat feeding increased serum leptin, HDL-C, and T-CHOL levels, while robustly elevating hepatic lipogenesis and lipid catabolism. A combination of TFA+MSG resulted in the highest levels of serum leptin, HDL-C, and T-CHOL, while reducing hepatic lipogenic gene expression and increasing markers of inflammation, lipid storage, DNA damage, and cell cycle impairment. In the adipocytes, Ppargc1a and REDOX gene expression were reduced compared with TFA alone, and several lipogenic genes were upregulated. Therefore, MSG augments *trans*-fat induced hepatic steatosis by altering WAT gene expression and elevating serum lipids and markers of hepatic fibrosis, inflammation, and DNA damage. Whether the MSG/TFA interaction is mirrored by other dietary fatty acids remains to be elucidated. Further investigation into the molecular pathology of diet-induced NAFLD should address the interaction between other dietary lipids and MSG.

The authors thank Rhea Mondreal and Mohammed Al-Halaby for technical assistance, the Comparative Medicine Department, King Faisal Specialist Hospital and Research Centre for animal husbandry, the Biological Repository Centre at King Faisal Specialist Hospital and Research Centre for histology work, and Mr. Hakim Al-Enazi for his unparalleled help in coordinating research resources.

REFERENCES

1. Targher, G. 2007. Non-alcoholic fatty liver disease, the metabolic syndrome and the risk of cardiovascular disease: the plot thickens. *Diabet. Med.* **24:** 1–6.
2. Luyckx, F. H., P. J. Lefebvre, and A. J. Scheen. 2000. Non-alcoholic steatohepatitis: association with obesity and insulin resistance, and influence of weight loss. *Diabetes Metab.* **26:** 98–106.
3. Solis-Herruzo, J. A., I. Garcia-Ruiz, M. Perez-Carreras, and M. T. Munoz-Yague. 2006. Non-alcoholic fatty liver disease. From insulin resistance to mitochondrial dysfunction. *Rev. Esp. Enferm. Dig.* **98:** 844–874.
4. Cave, M., I. Deaciuc, C. Mendez, Z. Song, S. Joshi-Barve, S. Barve, and C. McClain. 2007. Nonalcoholic fatty liver disease: predisposing factors and the role of nutrition. *J. Nutr. Biochem.* **18:** 184–195.
5. Dunn, W., and J. B. Schwimmer. 2008. The obesity epidemic and nonalcoholic fatty liver disease in children. *Curr. Gastroenterol. Rep.* **1:** 67–72.
6. Nobili, V., M. Marcellini, R. Devito, P. Ciampalini, F. Piemonte, D. Comparcola, M. R. Sartorelli, and P. Angulo. 2006. NAFLD in children: a prospective clinical-pathological study and effect of lifestyle advice. *Hepatology.* **44:** 458–465.
7. Yalniz, M., I. H. Bahçecioğlu, N. Kuzu, S. Celebi, H. Ataseven, B. Ustündağ, I. H. Ozercan, and K. Sahin. 2007. Amelioration of steatohepatitis with pentoxifylline in a novel nonalcoholic steatohepatitis model induced by high-fat diet. *Dig. Dis. Sci.* **52:** 2380–2386.
8. USDA Economic Research Service. Dietary Assessment of Major trends in US Food consumption, 1970–2005. http://www.ers.usda.gov/Publications/EIB33/EIB33_Reportsummary.pdf
9. Osso, F. S., A. S. Moreira, M. T. Teixeira, R. O. Pereira, M. G. Tavares do Carmo, and A. S. Moura. 2008. Trans fatty acids in maternal milk lead to cardiac insulin resistance in adult offspring. *Nutrition.* **24:** 727–732.
10. Saravanan, N., A. Haseeb, N. Z. Ehtesham, and Ghafoorunissa. 2005. Differential effects of dietary saturated and trans-fatty acids on expression of genes associated with insulin sensitivity in rat adipose tissue. *Eur. J. Endocrinol.* **153:** 159–165.
11. Astrup, A., J. Dyerberg, M. Selleck, and S. Stender. 2008. Nutrition transition and its relationship to the development of obesity and related chronic diseases. *Obes. Rev.* **1 (Suppl.):** 48–52.
12. Hirata, A. E., I. S. Andrade, P. Vaskevicius, and M. S. Dolnikoff. 1997. Monosodium glutamate (MSG)-obese rats develop glucose intolerance and insulin resistance to peripheral glucose uptake. *Braz. J. Med. Biol. Res.* **30:** 671–674.
13. de Mello, M. A., C. T. de Souza, L. R. Braga, J. W. dos Santos, I. A. Ribeiro, and C. A. Gobatto. 2001. Glucose tolerance and insulin action in monosodium glutamate (MSG) obese exercise-trained rats. *Physiol. Chem. Phys. Med. NMR.* **33:** 63–71.
14. Matyšková, R., L. Maletínská, J. Maixnerová, Z. Pirník, A. Kiss, and B. Železná. 2008. Comparison of the obesity phenotypes related to monosodium glutamate effect on arcuate nucleus and/or the high fat diet feeding in C57Bl/6 and NMRI mice. *Physiol. Res.* **57:** 727–734.

15. Larsen, P. J., J. D. Mikkelsen, D. Jessop, S. L. Lightman, and H. S. Chowdrey. 1994. Neonatal monosodium glutamate treatment alters both the activity and the sensitivity of the rat hypothalamo-pituitary-adrenocortical axis. *J. Endocrinol.* **141:** 497–503.
16. Nakanishi, Y., K. Tsuneyama, M. Fujimoto, T. L. Salunga, K. Nomoto, J. L. An, Y. Takano, S. Iizuka, M. Nagata, W. Suzuki, et al. 2008. Monosodium glutamate (MSG): a villain and promoter of liver inflammation and dysplasia. *J. Autoimmun.* **30:** 42–50.
17. FAO/WHO. 1974. Toxicological evaluation of certain food additives with a review of general pronciples and of specifications. 17th Report of the Joint FAO/WHO Expert Committee on Food Additives. FAO Nutrition Meetings Report Series no.53, WHO Technical Report Series no. 539.
18. Beyreuther, K., H. K. Biesalski, J. D. Fernstrom, P. Grimm, W. P. Hammes, U. Heinemann, O. Kempski, P. Stehle, H. Steinhart, and R. Walker. 2007. Consensus meeting: monosodium glutamate - an update. *Eur. J. Clin. Nutr.* **61:** 304–313.
19. Yoshida, T., K. Yoshioka, N. Sakane, T. Umekawa, and M. Kondo. 1995. Probucol prevents the progression of fatty liver in MSG obese mice. *Exp. Clin. Endocrinol. Diabetes.* **103:** 119–122.
20. Irizarry, R. A., B. Hobbs, F. Collin, Y. D. Beazer-Barclay, K. J. Antonellis, J. Scherf, and T. P. Speed. 2003. Exploration, normalization, and summaries of high density oligonucleotide array probe level data. *Biostatistics.* **4:** 249–264.
21. Tarling, E., A. Salter, and A. Bennett. 2004. Transcriptional regulation of human SREBP-1c (sterol-regulatory-element-binding protein-1c): a key regulator of lipogenesis. *Biochem. Soc. Trans.* **32:** 107–109.
22. Davis, R. A., J. H. Miyake, T. Y. Hui, and N. J. Spann. 2002. Regulation of cholesterol-7alpha-hydroxylase: BARElY missing a SHP. *J. Lipid Res.* **43:** 533–543.
23. Puri, V., S. Konda, S. Ranjit, M. Aouadi, A. Chawla, M. Chouinard, A. Chakladar, and M. P. Czech. 2007. Fat-specific protein 27, a novel lipid droplet protein that enhances triglyceride storage. *Biol. Chem.* **282:** 34213–34218.
24. Roden, M. 2006. Mechanisms of disease: hepatic steatosis in type 2 diabetes pathogenesis and clinical relevance. *Nat. Clin. Pract. Endocrinol. Metab.* **2:** 335–348.
25. Nwankwo, J. O., A. A. Spector, and F. E. Domann. 2003. A nucleotide insertion in the transcriptional regulatory region of FADS2 gives rise to human fatty acid delta-6-desaturase deficiency. *J. Lipid Res.* **44:** 2311–2319.
26. Deguchi, A., K. Segawa, K. Hosaka, I. B. Weinstein, and K. Umezawa. 2002. Overexpression of phosphatidylinositol synthase enhances growth and G1 progression in NIH3T3 cells. *Jpn. J. Cancer Res.* **93:** 157–166.
27. Larqué, E., P.A. García-Ruiz, F. Perez-Llamas, S. Zamora, and A. Gil. 2003. Dietary trans fatty acids alter the compositions of microsomes and mitochondria and the activities of microsome delta6-fatty acid desaturase and glucose-6-phosphatase in livers of pregnant rats. *J. Nutr.* **133:** 2526–2531.
28. Koh-Banerjee, P., N. F. Chu, D. Spiegelman, B. Rosner, G. Colditz, W. Willett, and E. Rimm. 2003. Prospective study of the association of changes in dietary intake, physical activity, alcohol consumption, and smoking with 9-y gain in waist circumference among 16,587 US men. *Am. J. Clin. Nutr.* **78:** 719–727.
29. Tetri, L. H., M. Basaranoglu, E. M. Brunt, L. M. Yerian, and B. A. Neuschwander-Tetri. 2008. Severe NAFLD with hepatic necroinflammatory changes in mice fed trans-fats and a high fructose corn syrup equivalent. *Am. J. Physiol. Gastrointest. Liver Physiol.* **295:** G987–G995.
30. Deng, Q. G., H. She, J. H. Cheng, S. W. French, D. R. Koop, S. Xiong, and H. Tsukamoto. 2005. Steatohepatitis induced by intragastric overfeeding in mice. *Hepatology.* **42:** 905–914.
31. Kohjima, M., M. Enjoji, N. Higuchi, M. Kato, K. Kotoh, T. Yoshimoto, T. Fujino, M. Yada, R. Yada, N. Harada, et al. 2007. Re-evaluation of fatty acid metabolism-related gene expression in nonalcoholic fatty liver disease. *Int. J. Mol. Med.* **20:** 351–358.
32. Sato, S., H. Shirakawa, S. Tomita, Y. Ohsaki, K. Haketa, O. Tooi, N. Santo, M. Tohkin, Y. Furukawa, F. J. Gonzalez, et al. 2008. Low-dose dioxins alter gene expression related to cholesterol biosynthesis, lipogenesis, and glucose metabolism through the aryl hydrocarbon receptor-mediated pathway in mouse liver. *Toxicol. Appl. Pharmacol.* **229:** 10–19.
33. Nebert, D. W., T. P. Dalton, A. B. Okey, and F. J. Gonzalez. 2004. Role of aryl hydrocarbon receptor-mediated induction of the CYP1 enzymes in environmental toxicity and cancer. *J. Biol. Chem.* **279:** 23847–23850.
34. Shaban, Z., S. El-Shazly, S. Abdelhady, I. Fattouh, K. Muzandu, M. Ishizuka, K. Kimura, A. Kazusaka, and S. Fujita. 2004. Down regulation of hepatic PPARalpha function by AhR ligand. *J. Vet. Med. Sci.* **66:** 1377–1386.
35. Donnelly, K. L., C. I. Smith, S. J. Schwarzenberg, J. Jessurun, M. D. Boldt, and E. J. Parks. 2005. Sources of fatty acids stored in liver and secreted via lipoproteins in patients with nonalcoholic fatty liver disease. *J. Clin. Invest.* **115:** 1343–1351.
36. Kohjima, M., N. Higuchi, M. Kato, K. Kotoh, T. Yoshimoto, T. Fujino, M. Yada, R. Yada, N. Harada, M. Enjoji, et al. 2008. SREBP-1c, regulated by the insulin and AMPK signaling pathways, plays a role in nonalcoholic fatty liver disease. *Int. J. Mol. Med.* **21:** 507–511.
37. Buettner, R., K. G. Parhofer, M. Woenckhaus, C. E. Wrede, L. A. Kunz-Schughart, J. Schölmerich, and L. C. Bollheimer. 2006. Defining high-fat-diet rat models: metabolic and molecular effects of different fat types. *J. Mol. Endocrinol.* **36:** 485–501.
38. Bykov, I., S. Junnikkala, M. Pekna, K. O. Lindros, and S. Meri. 2007. Effect of chronic ethanol consumption on the expression of complement components and acute-phase proteins in liver. *Clin. Immunol.* **124:** 213–220.
39. Liu, H. Y., Q. F. Collins, F. Moukdar, D. Zhuo, J. Han, T. Hong, S. Collins, and W. Cao. 2008. Suppression of hepatic glucose production by human neutrophil alpha-defensins through a signaling pathway distinct from insulin. *J. Biol. Chem.* **283:** 12056–12063.
40. Aranha, M. M., H. Cortez-Pinto, A. Costa, I. B. da Silva, M. E. Camilo, M. C. de Moura, and C. M. Rodrigues. 2008. Bile acid levels are increased in the liver of patients with steatohepatitis. *Eur. J. Gastroenterol. Hepatol.* **20:** 519–525.
41. Kagawa, S., T. Fujiwara, Y. Kadowaki, T. Fukazawa, R. Sok-Joo, J. A. Roth, and N. Tanaka. 1999. Overexpression of the p21 sdi1 gene induces senescence-like state in human cancer cells: implication for senescence-directed molecular therapy for cancer. *Cell Death Differ.* **6:** 765–772.
42. Richardson, M. M., J. R. Jonsson, E. E. Powell, E. M. Brunt, B. A. Neuschwander-Tetri, P. S. Bhathal, J. B. Dixon, M. D. Weltman, H. Tilg, A. R. Moschen, 2007. Progressive fibrosis in nonalcoholic steatohepatitis: association with altered regeneration and a ductular reaction. *Gastroenterology.* **133:** 80–90.
43. van der Poorten, D., K. L. Milner, J. Hui, A. Hodge, M. I. Trenell, J. G. Kench, R. London, T. Peduto, D. J. Chisholm, and J. George. 2008. Visceral fat: a key mediator of steatohepatitis in metabolic liver disease. *Hepatology.* **48:** 449–457.
44. Tchoukalova, Y. D., C. Koutsari, M. V. Karpyak, S. B. Votruba, E. Wendland, and M. D. Jensen. 2008. Subcutaneous adipocyte size and body fat distribution. *Am. J. Clin. Nutr.* **87:** 56–63.
45. Crunkhorn, S., F. Dearie, C. Mantzoros, H. Gami, W. S. da Silva, D. Espinoza, R. Faucette, K. Barry, A. C. Bianco, and M. E. Patti. 2007. Peroxisome proliferator activator receptor gamma coactivator-1 expression is reduced in obesity: potential pathogenic role of saturated fatty acids and p38 mitogen-activated protein kinase activation. *J. Biol. Chem.* **282:** 15439–15450.
46. Yoneda, M., K. Hotta, Y. Nozaki, H. Endo, T. Uchiyama, H. Mawatari, H. Iida, S. Kato, K. Hosono, K. Fujita, et al. 2008. Association between PPARGC1A polymorphisms and the occurrence of nonalcoholic fatty liver disease (NAFLD). *BMC Gastroenterol.* **8:** 27.
47. Leone, T. C., C. J. Weinheimer, and D. P. Kelly. 1999. A critical role for the peroxisome proliferator-activated receptor α (PPARα) in the cellular fasting response: the PPARα-null mouse as a model of fatty acid oxidation disorders. *Proc. Natl. Acad. Sci. USA.* **96:** 7473–7478.
48. Sprecher, D. L. 2007. Lipids, lipoproteins, and peroxisome proliferator activated receptor-delta. *Am. J. Cardiol.* **100:** n20–n24.
49. Finck, B. N., M. C. Gropler, Z. Chen, T. C. Leone, M. A. Croce, T. E. Harris, J. C. Lawrence, Jr., and D. P. Kelly. 2006. Lipin 1 is an inducible amplifier of the hepatic PGC-1alpha/PPARalpha regulatory pathway. *Cell Metab.* **4:** 199–210.
50. van Harmelen, V., M. Rydén, E. Sjölin, and J. Hoffstedt. 2007. A role of lipin in human obesity and insulin resistance: relation to adipocyte glucose transport and GLUT4 expression. *J. Lipid Res.* **48:** 201–206.
51. Horton, J. D., I. Shimomura, S. Ikemoto, Y. Bashmakov, and R. E. Hammer. 2003. Overexpression of sterol regulatory element-binding protein-1a in mouse adipose tissue produces adipocyte hypertrophy, increased fatty acid secretion, and fatty liver. *J. Biol. Chem.* **278:** 36652–36660.
52. Chui, P. C., H. P. Guan, M. Lehrke, and M. A. Lazar. 2005. PPARgamma regulates adipocyte cholesterol metabolism via oxidized LDL receptor 1. *J. Clin. Invest.* **115:** 2244–2256.